HAL
open science

The Net GHG Balance and Budget of the Permafrost Region (2000–2020) From Ecosystem Flux Upscaling

Justine Ramage, Mckenzie Kuhn, Anna-maria Virkkala, Carolina Voigt, Maija E Marushchak, Ana Bastos, Christina Biasi, Josep G Canadell, Philippe Ciais, Efrèn López-blanco, et al.

To cite this version:

Justine Ramage, Mckenzie Kuhn, Anna-maria Virkkala, Carolina Voigt, Maija E Marushchak, et al.. The Net GHG Balance and Budget of the Permafrost Region (2000–2020) From Ecosystem Flux Upscaling. Global Biogeochemical Cycles, 2024, 38 (4), 10.1029/2023gb007953 . hal-04536905

HAL Id: hal-04536905

https://hal.science/hal-04536905

Submitted on 8 Apr 2024

HAL is a multi-disciplinary open access archive for the deposit and dissemination of scientific research documents, whether they are published or not. The documents may come from teaching and research institutions in France or abroad, or from public or private research centers.

L'archive ouverte pluridisciplinaire **HAL**, est destinée au dépôt et à la diffusion de documents scientifiques de niveau recherche, publiés ou non, émanant des établissements d'enseignement et de recherche français ou étrangers, des laboratoires publics ou privés.

Check for updates

Global Biogeochemical Cycles

RESEARCH ARTICLE
10.1029/2023GB007953

Special Section:
RECCAP2

The Net GHG Balance and Budget of the Permafrost Region (2000–2020) From Ecosystem Flux Upscaling

Justine Ramage[1,2], McKenzie Kuhn[3], Anna-Maria Virkkala[1,4], Carolina Voigt[5], Maija E. Marushchak[6], Ana Bastos[7], Christina Biasi[6,8], Josep G. Canadell[9], Philippe Ciais[10], Efrèn López-Blanco[11], Susan M. Natali[4], David Olefeldt[12], Stefano Potter[4], Benjamin Poulter[13], Brendan M. Rogers[4], Edward A. G. Schuur[14], Claire Treat[15], Merritt R. Turetsky[16], Jennifer Watts[4], and Gustaf Hugelius[1,2]

[1]Department of Physical Geography, Stockholm University, Stockholm, Sweden, [2]Bolin Centre for Climate Research, Stockholm University, Stockholm, Sweden, [3]Department of Earth Sciences, University of New Hampshire, Durham, NH, USA, [4]Woodwell Climate Research Center, Falmouth, MA, USA, [5]Universität Hamburg, Institute of Soil Science, Hamburg, Germany, [6]Department of Environmental and Biological Sciences, University of Eastern Finland, Yliopistonranta 1 E, Kuopio, Finland, [7]Department of Biogeochemical Integration, Max Planck Institute for Biogeochemistry, Jena, Germany, [8]Department of Ecology, University of Innsbruck, Innsbruck, Austria, [9]Global Carbon Project, CSIRO Environment, Canberra, ACT, Australia, [10]Laboratoire des Sciences du Climat et de l'Environnement, LSCE-IPSL (CEA-CNRS-UVSQ), Université Paris-Saclay, Gif-sur-Yvette, France, [11]Department of Ecoscience, Arctic Research Center, Aarhus University, Roskilde, Denmark, [12]Department of Renewable Resources, University of Alberta, Edmonton, AB, Canada, [13]NASA GSFC, Biospheric Sciences Laboratory, Greenbelt, MD, USA, [14]Center for Ecosystem Science and Society, and Department of Biological Sciences, Northern Arizona University, Flagstaff, AZ, USA, [15]Alfred Wegener Institute Helmholtz Center for Polar and Marine Research, Potsdam, Germany, [16]Renewable and Sustainable Energy Institute, and Department of Ecology and Evolutionary Biology, University of Colorado, Boulder, CO, USA

Abstract The northern permafrost region has been projected to shift from a net sink to a net source of carbon under global warming. However, estimates of the contemporary net greenhouse gas (GHG) balance and budgets of the permafrost region remain highly uncertain. Here, we construct the first comprehensive bottom-up budgets of CO_2, CH_4, and N_2O across the terrestrial permafrost region using databases of more than 1000 in situ flux measurements and a land cover-based ecosystem flux upscaling approach for the period 2000–2020. Estimates indicate that the permafrost region emitted a mean annual flux of 12 (−606, 661) Tg CO_2–C yr^{-1}, 38 (22, 53) Tg CH_4–C yr^{-1}, and 0.67 (0.07, 1.3) Tg N_2O–N yr^{-1} to the atmosphere throughout the period. Thus, the region was a net source of CH_4 and N_2O, while the CO_2 balance was near neutral within its large uncertainties. Undisturbed terrestrial ecosystems had a CO_2 sink of −340 (−836, 156) Tg CO_2–C yr^{-1}. Vertical emissions from fire disturbances and inland waters largely offset the sink in vegetated ecosystems. When including lateral fluxes for a complete GHG budget, the permafrost region was a net source of C and N, releasing 144 (−506, 826) Tg C yr^{-1} and 3 (2, 5) Tg N yr^{-1}. Large uncertainty ranges in these estimates point to a need for further expansion of monitoring networks, continued data synthesis efforts, and better integration of field observations, remote sensing data, and ecosystem models to constrain the contemporary net GHG budgets of the permafrost region and track their future trajectory.

Plain Language Summary A quarter of the northern hemisphere is underlain by a permanently frozen ground called permafrost. This ground contains large amounts of carbon and nitrogen, making the permafrost region the largest terrestrial carbon and nitrogen pool on Earth. Due to unprecedented warming, permafrost thaws and reshapes landscapes, impacting their hydrology and biogeochemical cycling. This has the potential to increase the release of greenhouse gases such as carbon dioxide (CO_2), methane (CH_4), and nitrous oxide (N_2O) to the atmosphere, impacting the global climate. Although presumably crucial for the global carbon cycle, the role of the permafrost region in the global carbon budget is unknown. We present comprehensive budgets of CO_2, CH_4, and N_2O by key permafrost land cover types over the period 2000–2020 across the northern permafrost region. Estimates indicate that the permafrost region was emitting GHGs throughout the period. While the region was a source of methane and nitrous oxide, the carbon dioxide budget was near neutral with large uncertainties. Carbon dioxide emissions from wildfires and inland waters largely offset the sink in vegetated ecosystems. Uncertainties in estimates would be narrowed by increasing the number of in situ flux measurements in various ecosystems, sharpening ecosystem classifications, and integrating fluxes from disturbances.

Key Points:

- The region emitted 12 (−606, 661) Tg CO_2–C yr^{-1}, 38 (22, 53) Tg CH_4–C yr^{-1}, and 0.67 (0.07, 1.3) Tg N_2O–N yr^{-1} to the atmosphere between 2000 and 2020
- Based on the above, terrestrial ecosystems remained a CO_2 sink, but emissions from fires and inland waters largely offset the sink in vegetated ecosystems
- When also including lateral fluxes, the complete C and N budgets of the permafrost region result in net sources of 144 (−506, 826; including CO_2 and CH_4) Tg C yr^{-1} and 3 (2, 5) Tg N yr^{-1}

Supporting Information:

Supporting Information may be found in the online version of this article.

Correspondence to:

J. Ramage,
justine.ramage@natgeo.su.se

Citation:

Ramage, J., Kuhn, M., Virkkala, A.-M., Voigt, C., Marushchak, M. E., Bastos, A., et al. (2024). The net GHG balance and budget of the permafrost region (2000–2020) from ecosystem flux upscaling. *Global Biogeochemical Cycles*, *38*, e2023GB007953. https://doi.org/10.1029/2023GB007953

Received 11 SEP 2023
Accepted 29 FEB 2024

Author Contributions:

Conceptualization: McKenzie Kuhn, Anna-Maria Virkkala, Carolina Voigt, Maija E. Marushchak, Christina Biasi, Josep G. Canadell, Philippe Ciais, David Olefeldt, Benjamin Poulter, Brendan M. Rogers, Gustaf Hugelius
Data curation: McKenzie Kuhn, Anna-Maria Virkkala, Stefano Potter, Brendan M. Rogers, Gustaf Hugelius

© 2024. The Authors.
This is an open access article under the terms of the Creative Commons Attribution License, which permits use, distribution and reproduction in any medium, provided the original work is properly cited.

Formal analysis: McKenzie Kuhn, Anna-Maria Virkkala, Carolina Voigt, Maija E. Marushchak, Gustaf Hugelius
Funding acquisition: McKenzie Kuhn, Anna-Maria Virkkala, Carolina Voigt, Maija E. Marushchak, Christina Biasi, David Olefeldt, Brendan M. Rogers, Gustaf Hugelius
Investigation: McKenzie Kuhn, Anna-Maria Virkkala, Carolina Voigt, Maija E. Marushchak, Gustaf Hugelius
Methodology: McKenzie Kuhn, Anna-Maria Virkkala, Carolina Voigt, Maija E. Marushchak, David Olefeldt, Gustaf Hugelius
Project administration: Gustaf Hugelius
Resources: McKenzie Kuhn, Carolina Voigt, Maija E. Marushchak, Christina Biasi, David Olefeldt, Stefano Potter, Brendan M. Rogers, Gustaf Hugelius
Supervision: Gustaf Hugelius
Validation: McKenzie Kuhn, Anna-Maria Virkkala, Carolina Voigt, Maija E. Marushchak, Gustaf Hugelius
Visualization: McKenzie Kuhn, Anna-Maria Virkkala, Carolina Voigt, Maija E. Marushchak
Writing – original draft: McKenzie Kuhn, Anna-Maria Virkkala, Carolina Voigt, Maija E. Marushchak, David Olefeldt
Writing – review & editing: McKenzie Kuhn, Anna-Maria Virkkala, Carolina Voigt, Maija E. Marushchak, Ana Bastos, Christina Biasi, Josep G. Canadell, Philippe Ciais, Efrèn López-Blanco, Susan M. Natali, David Olefeldt, Stefano Potter, Benjamin Poulter, Brendan M. Rogers, Edward A. G. Schuur, Claire Treat, Merritt R. Turetsky, Jennifer Watts, Gustaf Hugelius

1. Introduction

The northern permafrost region covers up to 21 million km^2 of land in the Northern Hemisphere, of which ca. 70% (14 million km^2) is entirely underlain by permafrost (Obu et al., 2021)—ground that is at or below 0°C for at least two consecutive years. Unprecedented and amplified increases in air temperature in the Arctic (Rantanen et al., 2022) have strong impacts on the permafrost ground temperatures and extent (Biskaborn et al., 2019; Li et al., 2022), with future climate projections indicating a potential loss of permafrost extent of 4.0 ($-1.1 + 1.0$, 1σ confidence interval) million km^2 for each °C of global temperature change (Chadburn et al., 2017). Consequences are already visible, as ground temperatures near the depth of zero annual amplitude in the continuous permafrost zone increased by 0.39 ± 0.15 °C between 2007 and 2016, reducing the permafrost extent by 7% between 1969 and 2018 (Biskaborn et al., 2019; Li et al., 2022). Changes in ground temperature expose substantial quantities of organic carbon (C), resulting in C degradation and atmospheric release of greenhouse gases (GHGs) such as carbon dioxide (CO_2), methane (CH_4), and nitrous oxide (N_2O) from permafrost into the atmosphere (Chen et al., 2021; Natali et al., 2019; Schuur et al., 2009, 2015; Treat et al., 2018; Voigt et al., 2020a).

This release of GHGs to the atmosphere could have a strong impact on the global carbon cycle as the upper three m of permafrost region soils are estimated to store 1,000 ± 200 Pg (1 Pg = 1,000 Tg) of soil organic carbon (Hugelius et al., 2014; Mishra et al., 2021) and 55 Pg of soil nitrogen (N) (Palmtag et al., 2022). Deeper deposits store an additional 400–1,000 Pg C, making the permafrost region the largest terrestrial carbon and nitrogen pool on Earth (Schuur et al., 2022). These soil C and N have been accumulating over thousands of years due to limited microbial decomposition at low temperatures and water-logged conditions, leading to long-term accumulation of organic matter and incorporation into permafrost (Tarnocai et al., 2009). Upon thaw—that can occur gradually or abruptly—permafrost landscapes are changing, impacting their hydrology and biogeochemical cycling, creating a potentially significant feedback to the global climate (Schuur et al., 2008, 2015, 2022). The release of GHGs from permafrost has the potential to accelerate global climate warming, known as the "permafrost carbon feedback" (Burke et al., 2017, 2022; Schuur et al., 2015). While longer growing seasons, increased CO_2 concentrations, and additional nutrient release from thawing permafrost may lead to increased vegetation productivity and partly offset the release of permafrost GHGs (Koven et al., 2015; Liu, Kuhn, et al., 2022; López-Blanco et al., 2022; McGuire et al., 2018; Schuur & Mack, 2018), other processes such as disturbances cause rapid shifts to landscape structure (Schuur et al., 2008, 2011) and might accelerate the release of GHGs into the atmosphere.

Although presumably crucial for the global carbon cycle, the role of the northern permafrost region in the global carbon budget is unknown. Existing estimates of terrestrial GHG exchange from land cover-based or machine learning-based ecosystem vertical flux upscaling identify the northern permafrost terrestrial ecosystem as a net sink of CO_2 (-181 Tg CO_2–C yr^{-1}, Virkkala et al., 2021) and a net source of N_2O (0.14–1.03 Tg N_2O–N yr^{-1}, Voigt et al., 2020a), although large uncertainties remain. The northern permafrost region GHG budgets remain poorly constrained as our understanding of the GHG balance of this region has been hampered by low data availability (both temporal and spatial) and a heterogeneous landscape that is complex to map accurately. Watts et al. (2023) show that in northern high latitude, the Net Ecosystem Carbon Budget is reduced by ca. 7% when inland waters (e.g., lakes, ponds, streams, and rivers)—known to be significant emitters of CO_2 and CH_4 (Cole et al., 2007; Serikova et al., 2018; Stanley et al., 2016; Thornton et al., 2016; Wik et al., 2016)—are included, and by ca. 30% when emissions from inland waters and fires are considered. However, no study has yet included inland waters and disturbances to constrain the GHG budget of the permafrost region and provide an overall net GHG balance.

Here we fill this gap and present comprehensive budgets of GHGs (CO_2, CH_4, and N_2O) by key permafrost land cover types over the period 2000–2020 across the northern permafrost region using a single flux upscaling approach for all three GHGs. We include most relevant ecosystem components, that is, terrestrial ecosystems, inland waters, geological fluxes, lateral fluxes, and fire fluxes. However, we exclude direct anthropogenic emissions from the combustion of fossil fuels and land use change. The total carbon and nitrogen budgets that we provide for the region represent storage change budgets.

This permafrost regional budget is part of the REgional Carbon Cycle Assessment and Processes-2 (RECCAP2) project of the Global Carbon Project that aims to collect and integrate regional GHGs budgets for 12 land regions and 5 ocean basins covering all global lands and oceans (Ciais et al., 2022; https://www.globalcarbonproject.org/reccap/). Comparisons of GHG budgets using this upscaling flux approach and budgets based on atmospheric inversion models and terrestrial process-based models are discussed in Hugelius et al. (2023).

19449224, 2024, 4, Downloaded from https://agupubs.onlinelibrary.wiley.com/doi/10.1029/2023GB007953 by Cochrane France, Wiley Online Library on [08/04/2024]. See the Terms and Conditions (https://onlinelibrary.wiley.com/terms-and-conditions) on Wiley Online Library for rules of use; OA articles are governed by the applicable Creative Commons License

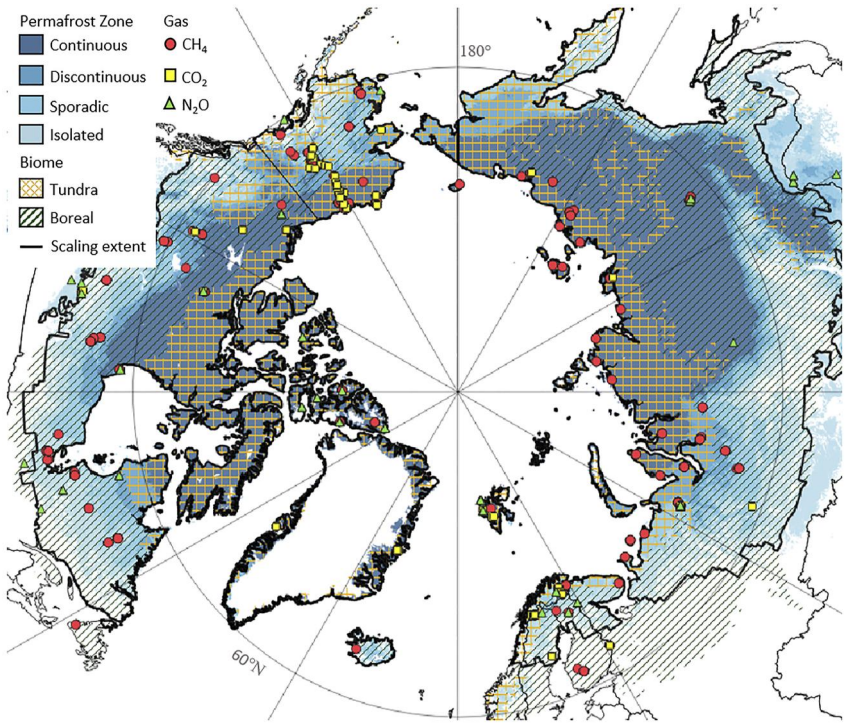

Figure 1. The BAWLD-RECCAP2 region defined as the northern permafrost extent (data from Obu et al., 2021) restricted to the Boreal Arctic Wetlands and Lakes Data set area (BAWLD, Olefeldt et al., 2021). The Figure overlays the extents of the Boreal Forests and the Tundra on the BAWLD-RECCAP2 region as well as the observation sites used for upscaling GHGs.

2. Materials and Methods

2.1. Study Area

The spatial extent of permafrost defined in this study includes areas within the northern permafrost region as defined in Obu et al. (2021) and restricted to the Boreal Arctic Wetlands and Lakes Data set area that had the key land cover classes for our upscaling (Boreal-Arctic Wetland and Lake Dataset (BAWLD), Olefeldt et al., 2021) (Figure 1). As a consequence, the BAWLD-RECCAP2 permafrost region does not include large areas underlain by permafrost in Central Asia and the Tibetan plateau (shown in Figure S1 in Supporting Information S1). The BAWLD-RECCAP2 permafrost region considered in this study is 18.5 million km^2. All flux estimates were scaled to the BAWLD-RECCAP2 permafrost region (hereafter permafrost region). The study area overlaps several other RECCAP2 regions (Ciais et al., 2022), and no specific effort to harmonize the budgets presented here with the RECCAP2 budgets of those regions is made in this paper.

2.2. GHG Budgets From Ecosystem Flux Upscaling

Data-driven ecosystem flux upscaling of GHG budgets for a reference time period of 2000–2020 was calculated by summing up flux budgets from terrestrial ecosystems, inland waters, lateral fluxes, fire emissions, and geological fluxes. To calculate the total net regional GHG flux (F_x), we used the following equation:

$$F_x = \sum_{j=1}^{j=n} A_j \times F_{jx}$$

where F_x is the annual permafrost region gas flux for the GHG species of interest x, A_j is the area of each land cover class j (Figure 2, Table S1), and F_{jx} is the land cover average GHG flux density for species x (Table S1).

We used existing synthesis databases and upscaled gridded data products published in the past 5 years to estimate annual and growing season mean fluxes per land cover type. All budget numbers are presented as the weight of C

19449224, 2024, 4, Downloaded from https://agupubs.onlinelibrary.wiley.com/doi/10.1029/2023GB007953 by Cochrane France, Wiley Online Library on [08/04/2024]. See the Terms and Conditions (https://onlinelibrary.wiley.com/terms-and-conditions) on Wiley Online Library for rules of use; OA articles are governed by the applicable Creative Commons License

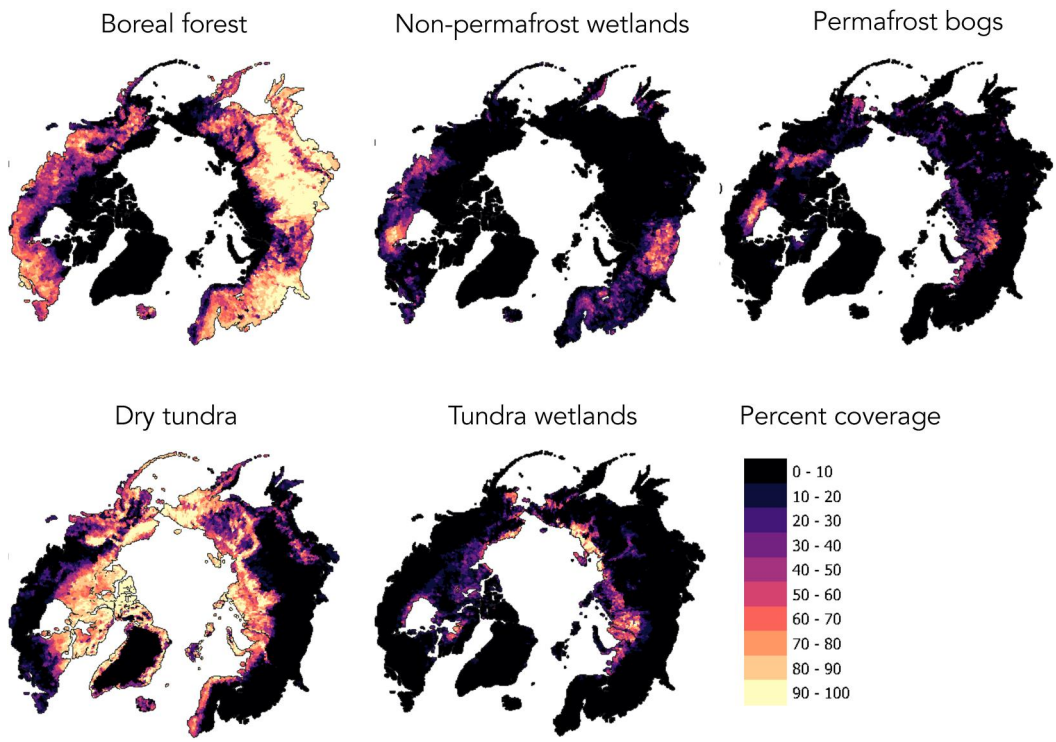

Figure 2. Circumpolar percentage coverage of the five adapted Boreal-Arctic Wetland and Lake Dataset (BAWLD) terrestrial land cover types (Boreal Forests, Non-permafrost Wetlands, Permafrost Bogs, Dry Tundra, and Tundra Wetlands) used for ecosystem-based upscaling of greenhouse gas flux budgets in this study. Note that these maps show the distributions across the full BAWLD domain as presented by Olefeldt et al. (2021), not the more limited extent of the RECCAP2 permafrost BAWLD domain used in this study.

and N (i.e., CO_2–C, CH_4–C and N_2O–N yr^{-1}) and not as the weight of GHG molecules. Budgets are reported as mean fluxes with uncertainties providing the 95% confidence intervals (CI) in Tg C or N.

2.3. GHG Fluxes From Terrestrial Land Cover Types

The land cover classification used for the analysis was adapted from the BAWLD set land cover (Olefeldt et al., 2021). The BAWLD land cover classes are distinguished based on moisture regime, nutrient/pH regime, organic-soil depth, hydrodynamics, and the presence or absence of permafrost (Olefeldt et al., 2021). To match the observational GHG flux data sets, we simplified the nine terrestrial land cover classes in BAWLD into five: Boreal Forests, Non-permafrost Wetlands, Dry Tundra, Tundra Wetlands, and Permafrost Bogs (Figure 2). Classes were defined as:

- *Non-permafrost Wetlands* include permafrost free bogs, fens, and marshes with no near-surface permafrost (see Canadian Wetland Classification system).
- *Boreal Forests* are forested ecosystems with non-wetland soils. Coniferous trees are dominant, but the class also includes deciduous trees in warmer climates and/or certain landscape positions. Boreal forest ecosystems may have permafrost or be permafrost free.
- *Permafrost Bogs* are ecosystems with near surface permafrost and thick surface peat layers (>40 cm). This includes palsas, peat plateaus, and the elevated portions of high- and low-center polygonal permafrost bogs. They typically have ombrotrophic conditions that cause nutrient-poor conditions. The vegetation is dominated by lichens, Sphagnum mosses, woody shrubs, and sometimes sparse coniferous forest.
- *Dry Tundra* include treeless ecosystems (both lowland arctic and alpine tundra) dominated by graminoid or shrub vegetation. Dry Tundra ecosystems generally have near-surface permafrost. Dry Tundra is differentiated from Permafrost Bogs by their thinner organic soil (<40 cm), and from Tundra Wetlands by their drained soils (average water table position >5 cm below soil surface).

19449224, 2024, 4, Downloaded from https://agupubs.onlinelibrary.wiley.com/doi/10.1029/2023GB007953 by Cochrane France, Wiley Online Library on [08/04/2024]. See the Terms and Conditions (https://onlinelibrary.wiley.com/terms-and-conditions) on Wiley Online Library for rules of use; OA articles are governed by the applicable Creative Commons License

- *Tundra Wetlands* are treeless ecosystems with near surface permafrost and saturated to inundated conditions for large parts of the year. Tundra Wetlands can both be mineral (<40 cm peat) or have peat (>40 cm peat). They are distinguished from Dry Tundra and Permafrost Bogs by being wetter and having more dynamic hydrology. Tundra Wetlands include areas that can be classified as tundra fen wetlands in the Canadian Wetland Classification System.

BAWLD was developed specifically to fit the needs of CH_4 upscaling and was dependent on available CH_4 flux data for different land cover classes. This choice of land cover classes was made after assessing the type of sites in three flux databases of CO_2, CH_4, and N_2O used for the upscaling (see description below), ensuring that there was sufficient data for each class and that the merging was the most parsimonious grouping that allowed us to estimate each GHG balance for each class. To match the observational GHGs data sets (see section below), we simplified wetland landcover classes for N_2O and CO_2 fluxes based on available flux data, related information on landcover classes, and differences in mechanistic drivers. For example, for N_2O fluxes, wetland classes were originally more coarsely separated into "peatlands" (>30 cm of organic layer) and "wetlands" (peatlands other than peatlands). Thus, N_2O Wetland fluxes were applied to the Tundra wetland and Marsh total areas, while N_2O Peatland fluxes were applied to the Bog, Fen, and Permafrost Bog total areas. For CH_4 upscaling, we kept the five wetland classes included in the work by Kuhn et al. (2021). Due to a lack of flux data, rocklands and glaciers were not included in the classification. The area of each land cover class (A_j) in km^2 across the permafrost region is shown in Figure 2 and detailed in Table S1.

The land cover mean GHG flux (F_{jx}) was obtained for each of the five terrestrial land cover classes after homogenizing and analyzing three comprehensive GHG flux data sets: Virkkala et al. (2022) for CO_2 fluxes; Kuhn et al. (2021a) for CH_4 fluxes; and Voigt et al. (2020a, 2020b) for N_2O fluxes. Additional data were extracted from the literature for Boreal Forest N_2O fluxes (Kim & Tanaka, 2003; Köster, Köster, Berninger, Heinonsalo, & Pumpanen, 2018; Matson et al., 2009; Morishita et al., 2007; Schiller & Hastie, 1996; Simpson et al., 1997; Ullah et al., 2009) since the N_2O flux data set from Voigt et al. (2020b) does not cover Boreal Forest ecosystems. These data sets comprise roughly 1,000 in situ growing-season and annual observations (including multiple observations from some sites) of terrestrial fluxes obtained from more than 200 sites using chamber (for CH_4, N_2O, and CO_2), diffusion (for CH_4 and CO_2), and eddy covariance (for CO_2 and CH_4) methods. The growing season length was defined as June to August (90 days) for the tundra and permafrost bogs sites, and May to September (150 days) for the boreal forests and non-permafrost wetlands. The CO_2 data set comprises year-round measurements of net ecosystem exchange (NEE), which we used to calculate the growing season and annual NEE. Average fluxes were calculated based on 93 sites and 403 observations for growing season NEE and 54 sites and 222 observations for annual NEE. The CH_4 and N_2O data sets provide growing-season measurements based on 98 sites and 458 observations of CH_4 exchange and 47 sites and 91 observations of N_2O exchange. For sites with incomplete growing season measurements, we multiplied average daily fluxes by the length of the growing season. Annual CH_4 fluxes were estimated assuming that growing season emissions accounted for 64% of annual emissions (Treat et al., 2018), except for boreal forests were we assumed growing season emissions accounted for 100% of annual emissions as the sites averaged net CH_4 growing season uptake and available data for winter season fractions only covers CH_4-emitting ecosystems (Treat et al., 2018). Therefore, our Boreal Forest annual estimate should be considered conservative. Annual N_2O fluxes were estimated assuming that growing season emissions accounted for 50% of annual emissions as reported in Voigt et al. (2020a). For all three GHGs, only sites with no record of large-scale upland hillslope abrupt thaw disturbance in the metadata were included in the flux estimates to avoid double-counting emissions from upland hillslope abrupt thaw (see methodology for disturbances). However, although scarce, we included other disturbed sites in our CO_2 estimates to account for ecosystem CO_2 losses following disturbances and their different successional stages (e.g., four sites reporting thermokarst; Virkkala et al., 2022). Sites from the above-mentioned GHG flux data sets were classified into one of the five terrestrial land cover classes using the metadata provided in each of the data sets.

While the focus of this study is the period 2000–2020, we include all in situ measurements obtained between 1991 and 2020 in order to overcome the limited amount of flux measurements in some of the ecosystems and therefore ensure adequate spatial representation of ecosystem fluxes. A separate analysis of decadal CO_2 fluxes from 1991 to 2020 revealed no differences, suggesting that the extension of the time series to 1991 does not impact our findings (Table S3).

19449224, 2024, 4, Downloaded from https://agupubs.onlinelibrary.wiley.com/doi/10.1029/2023GB007953 by Cochrane France, Wiley Online Library on [08/04/2024]. See the Terms and Conditions (https://onlinelibrary.wiley.com/terms-and-conditions) on Wiley Online Library for rules of use; OA articles are governed by the applicable Creative Commons License

More details on how ecosystem flux upscaling was performed (Text S1 in Supporting Information S1) as well as the temporal coverage of these data sets can be found in supplementary material (Figure S2 in Supporting Information S1, Table S2).

2.4. Vertical GHG Fluxes From Inland Waters

Similar to the method used to calculate GHG emissions from terrestrial land cover types, GHG fluxes from inland waters were calculated by upscaling mean GHG fluxes from lakes and rivers (see below) using the estimated surface area of these aquatic classes from the BAWLD classification (Olefeldt et al., 2021) adjusted to the study region (see supplementary Table S1 for estimated aerial extent of inland waters).

2.4.1. Vertical GHG Fluxes From Rivers

Atmospheric riverine GHG fluxes were calculated in different ways for each GHG, depending on available source data, and when possible scaled across the region using riverine area from the permafrost region (0.12×10^6 km^2), as reported in BAWLD.

Estimates of river and stream CO_2 flux were calculated from gridded monthly flux data estimated by Liu (2021; https://doi.org/10.5061/dryad.d7wm37pz9; Dryad) from river water dissolved CO_2 pressure and gas transfer velocity. This data is delivered as unprojected global grids with a 0.0083° resolution (which is ca 1×0.2 km pixels in the high Arctic). The global grids were clipped to the extent of BAWLD and then reprojected to an equal area grid at 100×100 m resolution. Vertical riverine fluxes were scaled across the riverine area in the domain BAWLD (0.12 10^6 km^2). Ice-free season river CO_2 emissions were calculated based on the mean-annual flux reported for the Arctic region by Liu, Kimball, et al. (2022). The river CO_2 flux reported by Liu, Kimball, et al. (2022) of 1,750 g C m^{-2} yr^{-1} incorporates the number of ice-free days; therefore, we scaled across the domain by multiplying the flux by the riverine area. To estimate total annual river CO_2 emissions—including emissions released after spring ice-out—we assumed that ice-out emissions accounted for 17% of annual emissions (Denfeld et al., 2018; consistent with the approach by Liu, Kimball, et al., 2022). Riverine CH_4 emissions were determined using the mean CH_4 diffusive flux reported in the MethDB (Stanley et al., 2016). Stanley et al. (2016) found that diffusive CH_4 emissions did not statistically differ across latitudes and scaled global river CH_4 emissions using one mean value. Given the limited number of reported CH_4 fluxes for rivers in the Arctic, we used the same approach as Stanley et al. (2016) and applied a global mean diffusive flux of 135 mg CH_4 m^{-2} d^{-1} to the river area. Because there are few studies that measure CH_4 emissions upon ice-out, we applied for CH_4 the same estimate as for CO_2, where 17% of annual fluxes occur during the ice-free period (Denfeld et al., 2018; consistent with the approach by Liu, Kuhn, et al., 2022). Ebullition was not included for river CH_4 emission estimates due to few available measurements in the literature for this region (Stanley et al., 2016). Estimates of river N_2O flux were derived from gridded annual N_2O flux estimated by a mechanistic mass balance model developed globally for inland waters by Maavara et al. (2019). These data were reprojected from an original 0.5° unprojected grid to an equal area grid at 1 km resolution and clipped to the BAWLD extent. As the original lake and river surface area was not known, no correction of the inland water surface area was made.

Uncertainties for river GHG balance were determined using the standard error and coefficient of variance reported by Liu, Kuhn, et al. (2022), Stanley et al. (2016) and Maavara et al. (2019), respectively, for CO_2, CH_4, and N_2O.

2.4.2. Vertical GHG Fluxes From Lakes

CH_4 fluxes (diffusion and ebullition) were extracted from the BAWLD-CH4 aquatic ecosystem data set and classified based on classes (yedoma lakes, peatland ponds, and glacial/post-glacial organic poor lakes and ponds) and sizes, from large (>10 km^2) to midsize (0.1–10 km^2) to small lakes (<0.1 km^2) (Kuhn et al., 2021a; total area = 1.255 10^6 km^2; Table S4). As in Olefeldt et al. (2021) any area -regardless of its size - which is likely to be inundated >50% of the growing season period (long term average) is considered part of the lake land cover classes. Ice-free days were determined based on averages of reported ice-free days for each lake type and this information was used to determine ice-free season fluxes (supplementary Table S1). In addition to ice-free emissions, spring ice-out emissions (i.e., winter contribution) were considered to be 23% of the annual total (Wik et al., 2016).

19449224, 2024, 4, Downloaded from https://agupubs.onlinelibrary.wiley.com/doi/10.1029/2023GB007953 by Cochrane France, Wiley Online Library on [08/04/2024]. See the Terms and Conditions (https://onlinelibrary.wiley.com/terms-and-conditions) on Wiley Online Library for rules of use; OA articles are governed by the applicable Creative Commons License

Estimated lake CO_2 fluxes were compiled from multiple available sources based on a literature search made in May 2022 (Humborg et al., 2010; Karlsson et al., 2013; Kortelainen et al., 2006; Pelletier et al., 2014; Rasilo et al., 2015; Rocher-Ros et al., 2017; Sepulveda-Jauregui et al., 2015) and are summarized in Table S5). The studies report lake CO_2 fluxes as mean flux values for various binned lake surface areas. We took these averages and grouped them by the lake size classes included in BAWLD (<0.1, 0.1–10, >10 km^2). We found no statistical differences in fluxes between the size groups and thus used one mean lake CO_2 flux to scale across the year and the region (315 ± 196 mg C m^{-2} d^{-1}). We applied the same number of ice-free days used to scale lake CH_4 emissions (ice-free days reported in the literature for each lake class).

To estimate lake fluxes of N_2O, gridded global data of annual flux from Lauerwald et al. (2019) were used. This estimate is based on the nitrous oxide (N_2O) emission model developed by Maavara et al. (2019) and the HydroLAKES database and was reprojected from an original 0.5° unprojected grid to an equal area grid at 1 km resolution and clipped to the BAWLD extent. As the original lake and river surface area was not known, no correction of the inland water surface area was made. Uncertainties for lake N_2O were determined using the coefficient of variance reported for regions north of 50° latitude in Lauerwald et al. (2019).

2.5. Disturbances—GHG Fluxes From Fires and Abrupt Thaw

Monthly GHG fire emissions were extracted for the study region from the Global Fire Emission Database version 4s for the period 1997–2016 and its Beta version for the years 2017–2020 (GFED; van der Werf et al., 2017). The GFED4s estimates of burned areas are based on remote sensing data at a spatial resolution of 0.25° (van der Werf et al., 2017). GHG emissions in the GFED4s are derived from the multiplication of burned area and fuel consumption per unit burned area, the latter being the product of modeled fuel loads per unit area and combustion completeness. For our purpose, we extracted mean annual GHG emissions from burned areas using the GFED4s for the period 2000–2016 and the GFED4s Beta for the period 2017–2020. To validate the use of the GFED4s Beta for the later period we compared the emissions obtained with the ones by van Wees et al. (2022) (Figure S3 in Supporting Information S1).

Localized, but widespread, disturbances associated with abrupt thaw are thought to contribute significantly to GHG emissions from permafrost (Abbott & Jones, 2015; Holloway et al., 2020; Marushchak et al., 2021; Runge et al., 2022; Turetsky et al., 2020; Walker et al., 2019; Yang et al., 2018). Abrupt thaw includes thawing processes that affect permafrost soils in periods of days to several years (Grosse et al., 2011), and is typically associated with thermokarst and thermoerosion processes that lead to the formation of hillslope erosional features (thaw slumps, thermo-erosion gullies and active layer detachments), thermokarst lakes, and thermokarst wetlands (i.e., collapse scar bogs and fens). We report abrupt thaw areas and derived annual CO_2 and CH_4 emissions using the inventory-based abrupt thaw model by Turetsky et al. (2020), in which atmospheric emissions are estimated for three generalized types of abrupt thaw terrains: mineral-rich lowlands, upland hillslopes, and organic-rich wetlands. In the abrupt thaw model, abrupt thaw areas are based on synthesized field observations and remote sensing measurements. GHG emissions from abrupt thaw were synthesized for each ecosystem state within each abrupt thaw type from the literature (ca. 20 published papers). The abrupt thaw model was initialized for a historical assessment period (1900–2000) to provide the model with a spin up and prevent the regional carbon fluxes starting at zero at the beginning of the dynamic measurement period. Thaw rates were generally in equilibrium with succession and recovery of surface permafrost during this initialization period. Changes in the area of each successional state were tracked over time by multiplying initial starting areas by transition rates. Estimates of abrupt thaw GHG emissions following the historical assessment period were performed by increasing rates of abrupt thaw through time. This increase in thaw rate was prescribed to follow the average output of "permafrost-enabled" land surface models, all of which were forced by atmospheric climate anomalies from the Community Climate System Model 4 Earth system model under an RCP8.5 projection. For our purpose, we ran the abrupt thaw model for the period 2000–2020, extracted cumulative CO_2 and CH_4 emissions from active and stabilized abrupt thaw features, and derived annual fluxes for each abrupt thaw terrain for the time period 2000–2020. We used the reported uncertainty ranges of ±40% on the upland hillslope areas, ±30% on the mineral-rich lowland areas, and ±35% on the organic-rich wetland areas, as in Turetsky et al. (2020). Additional details on the inventory model can be found in Turetsky et al. (2020). Since GHG data sets that we used for ecosystem upscaling partly account for abrupt thaw and to prevent double counting of GHG fluxes, CO_2 and CH_4 fluxes from abrupt thaw were added as a sub-flux (not added to the total) of terrestrial and inland water land cover fluxes and their

19449224, 2024, 4, Downloaded from https://agupubs.onlinelibrary.wiley.com/doi/10.1029/2023GB007953 by Cochrane France, Wiley Online Library on [08/04/2024]. See the Terms and Conditions (https://onlinelibrary.wiley.com/terms-and-conditions) on Wiley Online Library for rules of use; OA articles are governed by the applicable Creative Commons License

contribution to the total GHG budget is discussed. Due to the lack of in situ observations of abrupt thaw impacts on N_2O fluxes in the used data sets, no N_2O balance is presented for abrupt thaw.

2.6. Lateral Fluxes and Geological Emissions

Lateral C and N fluxes from riverine transport and coastal erosion (i.e., dissolved organic carbon (DOC) and dissolved organic nitrogen (DON) losses from the permafrost region to the ocean) are taken from Terhaar et al. (2021), representative for all land north of 60° N. They estimated riverine lateral fluxes for the six largest Arctic rivers (Mackenzie, Yukon, Kolyma, Lena, Ob, Yenisei) from the Arctic Great River Observatory data set and extrapolated them to the entire Arctic catchment. Emissions from coastal erosion were calculated by multiplying spatially resolved estimates of coastal erosion rates by estimates of C content in coastal soils provided by Lantuit et al. (2012).

Estimates of geological emissions of CH_4 (from subsurface fossil hydrocarbon reservoirs) are taken from an upscaled circumpolar permafrost region estimate for gas seeps along permafrost boundaries and lake beds made by Walter Anthony et al. (2012). We note that there is some risk of double counting such fluxes, especially in sites where eddy covariance flux towers may have unknowingly been placed close to seeps of geological CH_4 emissions. No separate estimates of geological emission for CO_2 or N_2O are available for the permafrost region. For CO_2, the full global geological emissions are estimated to 0.16 Pg CO_2–C yr^{-1} (Mörner & Etiope, 2002).

3. Results and Discussion

3.1. Net GHG Balance From Terrestrial Land Cover Types

Terrestrial ecosystems represent a decadal-scale sink for CO_2 and source for CH_4 and N_2O (Table 1, Figure 3). The mean annual CO_2 flux was a net sink, but could not be distinguished from CO_2 neutral when the 95% confidence interval was considered (−339.6 (−835.5, 156.3) Tg CO_2–C yr^{-1}). The broad uncertainty interval can be attributed both to the large natural variability in CO_2 fluxes across sites and to the heterogeneity of ecosystem types included in each of the land cover classes defined in the BAWLD classification. Boreal Forests and Non-permafrost Wetlands were CO_2 sinks (−270.3 and −69.4 Tg CO_2–C yr^{-1}, respectively), while Tundra Wetlands and Permafrost Bogs were close to neutral (−2.7 and −0.05 Tg CO_2–C yr^{-1}, respectively). Dry Tundra was the only ecosystem type classified as an annual ecosystem CO_2 source (2.9 Tg CO_2–C yr^{-1}), but the very broad uncertainty range (−147.6, 153.5 Tg CO_2–C yr^{-1}) indicates low confidence in the sign of this flux. Terrestrial ecosystems were overall a net sink of CO_2 during the growing season (−1,611 (−2148, −1,074) Tg CO_2–C gs^{-1}), with the strongest sink in the boreal forest (−1,034 (−1,305, −763) Tg CO_2–C gs^{-1}) (Table 2).

Annual vertical terrestrial CO_2 balance has been reported for high-latitudes in recent papers using different upscaling approaches. While closely related due to overlap in flux data, a higher NEE uptake is reported by both Virkkala et al. (2021) and Watts et al. (2023) (−419 (95% CI of −559 to −189) Tg CO_2–C yr^{-1} and −601 (standard error of ±1138) Tg CO_2–C yr^{-1}, respectively). However, the estimated NEE uptakes for the permafrost region solely are weaker, with an uptake of −181 (−305, 32) Tg CO_2–C yr^{-1} and −230 (±22) Tg CO_2–C yr^{-1}, respectively). The difference between the later NEE uptakes and our results relates to the subset of data included in the analyses (exclusively eddy covariance tower fluxes in Watts et al., 2023), the different years covered in the analyses (Virkkala et al., 2021: 1990–2015, Watts et al., 2023: 2003–2015), the different spatial extents, and the upscaling approach applied (Arctic Terrestrial Carbon Flux Model (TCFM-Arctic) in Watts et al., 2023, and statistical upscaling in Virkkala et al., 2021). Both of these studies as well as the previous RECCAP synthesis (1990–2006, McGuire et al., 2012) report the tundra as a weak CO_2 sink (−13 (−81, 62); −16 (±84–270); and −16 (−42, 10) Tg CO_2–C yr^{-1}, respectively) although they also show that annual tundra CO_2 balance cannot be distinguished from CO_2 neutral when taking into account the uncertainty range. Dry Tundra CO_2 balance was also identified as a source of 10 (−27, 47) Tg CO_2–C yr^{-1} in McGuire et al. (2012).

Our estimated annual net CH_4 source of 25.6 (14.7, 36.4) Tg CH_4–C yr^{-1} from terrestrial ecosystems (Table 1) was largely driven by emissions from Non-permafrost Wetlands (20.6 (14.3, 26.9) Tg CH_4–C yr^{-1}). As in Treat et al. (2018), Non-permafrost Wetlands emitted more than Tundra Wetlands. Annual CH_4 flux estimates for Tundra Wetlands (3.3 (2.7, 3.9) Tg CH_4 yr^{-1}) and Dry Tundra (2.1 (−0.4, 4.5 Tg CH_4–C yr^{-1}) were in the lower range from the previous estimates provided by McGuire et al. (2012), in which the tundra was estimated to release 11 (0, 22) Tg CH_4–C yr^{-1} (between 1990 and 2006). Our growing season CH_4 budget was a source of 16 (8.6,

19449224, 2024, 4, Downloaded from https://agupubs.onlinelibrary.wiley.com/doi/10.1029/2023GB007953 by Cochrane France, Wiley Online Library on [08/04/2024]. See the Terms and Conditions (https://onlinelibrary.wiley.com/terms-and-conditions) on Wiley Online Library for rules of use; OA articles are governed by the applicable Creative Commons License

Table 1
Greenhouse gas (GHGs–CO_2, CH_4, and N_2O) Balance and Total C and N Budgets for the Permafrost Region Based on Ecosystem Flux Upscaling

	Area	CO_2			CH_4			N_2O		
		Tg CO_2–C yr^{-1}			Tg CH_4–C yr^{-1}			Tg N_2O–N yr^{-1}		
	10^6 km^2	Mean	2.5% CI	97.5% CI	Mean	2.5% CI	97.5% CI	Mean	2.5% CI	97.5% CI
Upland and wetland land covers	17.05	**−339.59**	−835.5	156.3	**25.6**	14.7	36.4	**0.55**	−0.03	1.1
Boreal Forests	9	**−270.32**	−539.8	−0.9	**−1.1**	−2.2	0.0	**0.14**	−0.01	0.30
Non-permafrost Wetlands	1.6	**−69.4**	−124.7	−14.2	**20.6**	14.3	26.9	**0.07**	−0.03	0.17
Permafrost Bogs	0.86	**−0.05**	−0.82	0.73	**0.7**	0.3	1.1	**0.10**	−0.03	0.23
Dry Tundra	5.2	**2.9**	−147.6	153.5	**2.1**	−0.4	4.5	**0.23**	0.04	0.42
Tundra Wetlands	0.38	**−2.7**	−22.6	17.2	**3.3**	2.7	3.9	**0.01**	0.00	0.02
Subfraction from wetland abrupt thaw[a]	*0.72*	***19.3***	*12.6*	*26.1*	***19.05***	*12.4*	*25.7*	*NA*	*NA*	*NA*
Subfraction from upland hillslope abrupt thaw[a]	*0.014*	***0.3***	*0.2*	*0.5*	***4.1***	*2.4*	*5.7*	*NA*	*NA*	*NA*
Inland waters	1.4	**230.6**	132.4	359.8	**9.4**	4.5	13.1	**0.0019**	0.0008	0.0029
Rivers	0.12	**164.4**	107.3	222.5	**2.3**	1.6	2.9	**0.0006**	0.0004	0.0008
Lakes	1.3	**66.2**	25.1	137.3	**7.1**	2.9	10.2	**0.0012**	0.0004	0.002
Subfraction from lowland abrupt thaw lakes[a]	0.43	**11.6**	8.2	15.1	**7.8**	5.5	10	NA	NA	NA
Fires	1.1	**121.0**	96.7	145.3	**1.8**	1.4	2.1	**0.12**	0.10	0.15
Boreal	0.96	**111.0**	87.7	134.3	**1.6**	1.3	2.0	**0.113**	0.089	0.137
Tundra	0.11	**9.4**	5.5	13.3	**0.14**	0.08	0.20	**0.009**	0.005	0.014
Geological emissions		NA	NA	NA	**1.5**	1.2	1.8	NA	NA	NA
Total GHG balance		**11.98**	−606.4	661.4	**38.3**	21.8	53.4	**0.67**	0.07	1.25
Lateral fluxes		**94**	79	111	NA	NA	NA	**2.6**	1.9	3.6
Riverine flux		**78**	70	87				**1.0**	0.9	1.1
Coastal erosion		**15**	9.2	24				**1.6**	1.0	2.5
Total C[b] and N budgets		**106.0**	−527.4	772.4				**3.3**	2.0	4.8

Note. Negative GHG emissions represent an uptake while positive emissions represent a release. GHG emissions from terrestrial ecosystems are reported as mean fluxes with 2.5 and 97.5% confidence intervals (CI). GHG emissions from inland waters and fires are reported with 5 and 95% CI. GHG emissions from abrupt thaw are reported with ±40% uncertainty range. Bold values were to emphasize the columns with the mean values. [a]These fluxes are estimated using the abrupt thaw model from Turetsky et al. (2020) and are considered as additive to the total for these categories (to avoid double counting of fluxes). [b]Includes CO_2, CH_4, and lateral fluxes.

23.3) Tg CH_4–C gs^{-1} (Table 2), with non-permafrost Wetlands contributing 83%. All terrestrial ecosystems except Boreal Forests were net CH_4 emitters. Boreal Forests were a net sink of CH_4 (−1.1 (−2.3, 0.0) Tg CH_4–C gs^{-1}). This net CH_4 uptake from Boreal Forests was shown in a synthesis of site-level and plot-level CH_4 on the order of −1.1 mg CH_4 m^{-2} d^{-1} (Kuhn et al., 2021). This is largely driven by net CH_4 oxidation in the aerobic soils, many of which are covered by forest (non-Sphagnum) mosses. Moreover, recent investigations of the regulatory mechanisms of CH_4 oxidation in Boreal Forests show evidence that SOC constitutes an important variable that governs the forest CH_4 sink by providing alternative carbon compounds for methanotrophs and enhancing their activity by stimulating growth (Lee et al., 2023). The net sink of atmospheric CH_4 in well-drained soils is widely recognized in global budgets (e.g., Saunois et al., 2019) as well as in earlier process-based studies (Whalen et al., 1992). Our CH_4 annual balance was lower than those estimated for the northern high latitude wetlands (>45°N) at 31, 32, and 35 Tg CH_4−C yr^{-1} (depending on wetland distribution maps) by Peltola et al. (2019) and 38 Tg CH_4−C yr^{-1} by Watts et al. (2023). However, our CH_4 growing season balance estimate was higher than the balance based on 93 observations presented in Treat et al. (2018) except for the Tundra Wetlands where they remain within the same range. Despite their large spatial coverage, the Dry Tundra was a small source of CH_4 during the growing season (1.4 (−0.3, 2.9) Tg CH_4–C gs^{-1}), although the low end of the CI suggests that it could remain a sink. More measurements from these drier ecosystems are needed, as also recent studies indicate that tundra soils, in particular well-drained uplands, could be important CH_4 sinks (D'Imperio et al., 2023; Oh et al., 2020; Voigt et al., 2023).

19449224, 2024, 4, Downloaded from https://agupubs.onlinelibrary.wiley.com/doi/10.1029/2023GB007953 by Cochrane France, Wiley Online Library on [08/04/2024]. See the Terms and Conditions (https://onlinelibrary.wiley.com/terms-and-conditions) on Wiley Online Library for rules of use; OA articles are governed by the applicable Creative Commons License

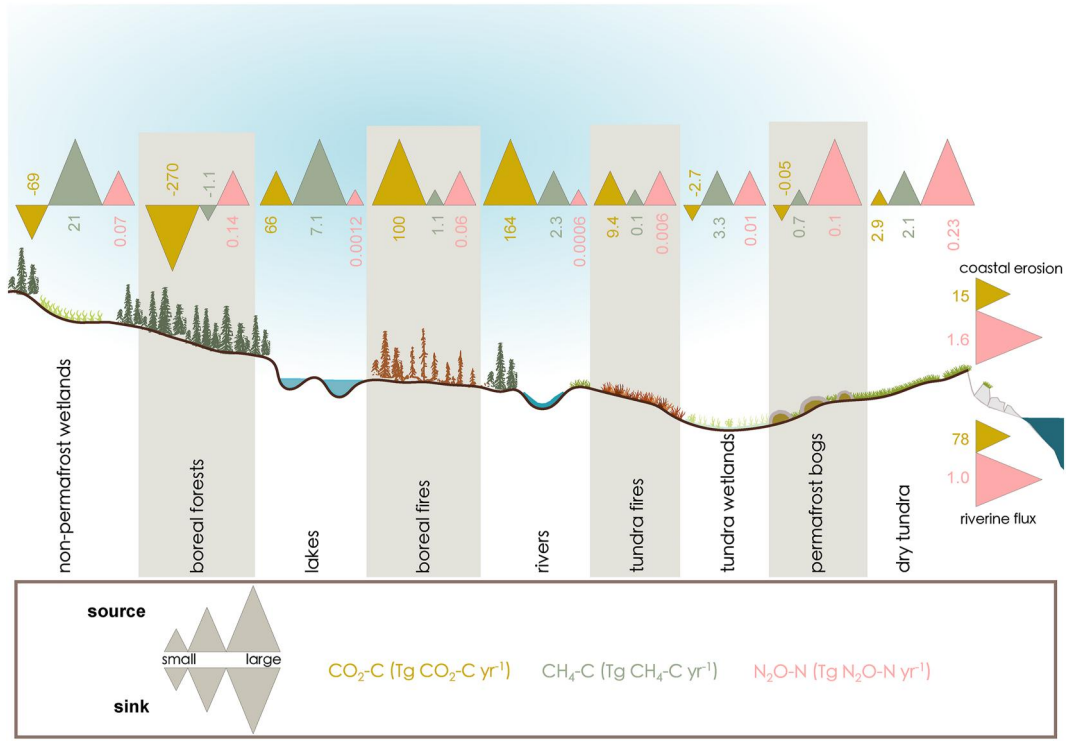

Figure 3. Scheme of annual atmospheric greenhouse gases (GHGs) exchange (CO_2, CH_4, and N_2O) for the five terrestrial land cover classes (Boreal Forests (9.0×10^6 km^2), Non-permafrost Wetlands (1.6×10^6 km^2), Dry Tundra (5.2×10^6 km^2), Tundra Wetlands (0.4×10^6 km^2) and Permafrost Bogs (0.9×10^6 km^2)); inland water classes (Rivers (0.1×10^6 km^2) and Lakes (1.3×10^6 km^2)). Annual lateral fluxes from coastal erosion and riverine fluxes are also reported in Tg C yr^{-1} and Tg N yr^{-1}. Symbols for fluxes indicate high (x > Q3), medium (Q1 < x < Q3), and low (<Q1) fluxes, in comparison with the quartile (Q). Note that the magnitudes across three different GHG fluxes within each land cover class cannot be compared with each other.

Our N_2O annual balance estimate of 0.55 (−0.03, 1.1) Tg N_2O–N yr^{-1} (Table 1) suggests that terrestrial ecosystems were a N_2O source, although the uncertainty range around N_2O fluxes extends from a small sink to a larger source. These high uncertainties partly relate to the limited number of observations of N_2O fluxes (47 sites and 91 observations), which only include growing-season observations. Our estimated annual N_2O balance is within the range of the one previously reported by Voigt et al. (2020a) (0.14–1.03 Tg N_2O–N yr^{-1} median-mean-based estimate). In our study, Dry Tundra was the largest N_2O source (0.23 (0.04, 0.42) Tg N_2O–N yr^{-1}). Boreal

Table 2
Growing Season (gs) Emissions of Greenhouse Gas (GHGs–CO_2, CH_4, and N_2O) From Terrestrial Ecosystems in the Permafrost Region

	Area		CO_2				CH_4				N_2O		
			Tg CO_2–C gs^{-1}				Tg CH_4–C gs^{-1}				Tg N_2O–N gs^{-1}		
	10^6 km^2	Sites (#)	Mean	2.5% CI	97.5% CI	Sites (#)	Mean	2.5% CI	97.5% CI	Sites (#)	Mean	2.5% CI	97.5% CI
Upland and wetland land covers	17.05	95	**−1,611**	−2148	−1,074	458	**16**	8.6	23.3	45	**0.273**	−0.019	0.572
Boreal Forests	9	25	**−1,034**	−1,305	−763	26	**−1.1**	−2.3	0	13	**0.07**	−0.01	0.15
Non-permafrost Wetlands[a]	1.6	10	**−145**	−193	−96	182	**13**	9.1	17	11	**0.03**	−0.02	0.09
Permafrost Bogs	0.86	2	**−54**	−139	31	79	**0.50**	0.20	0.70	5	**0.05**	−0.01	0.11
Dry Tundra	5.2	25	**−358**	−482	−234	62	**1.4**	−0.3	2.9	16	**0.11**	−0.02	0.21
Tundra Wetlands	0.38	33	**−20**	−29	−234	109	**2.1**	1.7	25	11	**0.01**	0.00	0.01

Note. GHG emissions are reported as mean fluxes with 2.5 and 97.5% confidence intervals (CI). [a]Non-permafrost Wetlands include fens, bogs, and marshes. Due to lack of data, N_2O fluxes for non-permafrost Wetlands, fluxes are assumed to be equal to those of Tundra Wetlands.

19449224, 2024, 4, Downloaded from https://agupubs.onlinelibrary.wiley.com/doi/10.1029/2023GB007953 by Cochrane France, Wiley Online Library on [08/04/2024]. See the Terms and Conditions (https://onlinelibrary.wiley.com/terms-and-conditions) on Wiley Online Library for rules of use; OA articles are governed by the applicable Creative Commons License

Forests were the second largest N_2O source (0.14 (−0.01, 0.30) Tg N_2O–N yr^{-1}) due to their large area, although their fluxes per unit area were small (Table S6, 52.43 μg N_2O m^{-2} d^{-1}). Although they occupy a small portion of the landscape (5%), Permafrost Bogs were the largest N_2O emitters per unit area (Table S6, 645.14 μg N_2O m^{-2} d^{-1}) and their contribution to the regional N_2O balance was 18%. The estimate for Permafrost Bogs includes emissions from barren peat surfaces, where vascular plants are absent - surfaces previously identified as N_2O hot spots in the Arctic due to ideal conditions for N_2O production (Gil et al., 2022; Marushchak et al., 2011; Repo et al., 2009). A challenge remains regarding the mapping of Permafrost Bogs and barren ground and integration within land cover classifications. Therefore, we did not differentiate between vegetated and non-vegetated Permafrost Bog areas when upscaling. N_2O emissions from Tundra Wetlands were negligible (0.01 (0.00, 0.02) Tg N_2O–N yr^{-1}), which can be explained by the lack of nitrate supply as an N_2O precursor under reduced conditions and reduction of N_2O to N_2 during denitrification when the water table is high (Butterbach-Bahl & Dannenmann, 2011; Voigt et al., 2017). Recent observations not included in the N_2O review data set (Voigt et al., 2020a) show that wetlands may also function as net N_2O sinks in the Arctic (Schulze et al., 2023).

3.2. Net GHG Balance From Inland Waters

Inland aquatic ecosystems were a net source of CO_2 (230.6 (132.4, 359.8) Tg CO_2–C yr^{-1}), CH_4 (9.4 (4.5, 13.1) Tg CH_4–C yr^{-1}), and N_2O (0.0019 (0.0008, 0.0029) Tg N_2O–N yr^{-1}). Rivers annually emit 164.4 (107.3, 222.5) Tg CO_2–C yr^{-1}, 2.3 (1.6, 2.9) Tg CH_4–C yr^{-1} and 0.0006 (0.0004, 0.0008) Tg N_2O–N yr^{-1} to the atmosphere. These high riverine fluxes are due to their supersaturation in CO_2 as they receive and degass CO_2 derived from adjacent soils. To our knowledge, there are no specific annual estimates of riverine GHGs for the permafrost region to compare our estimates; however, when compared to emissions from high latitudes, our CH_4 emissions for rivers are within the lower range of published estimates (0.3–7.5 Tg CH_4–C yr^{-1}) (Thornton et al., 2016).

In comparison to riverine emissions, lakes were a weaker source of CO_2 (66.2 (25.1, 137.3) Tg CO_2–C yr^{-1}) but a stronger source of CH_4 (7.1 (2.9, 10.2) Tg CH_4 yr^{-1}) and N_2O (0.0012 (0.0004, 0.002) Tg N_2O–N yr^{-1}) (Table 1). Our annual lake CH_4 emission estimate is lower than previous estimates reported by Wik et al. (2016) (12.4 (7.3, 25.7) Tg CH_4–C yr^{-1}) and Matthews et al. (2020) (13.8–17.7 Tg CH_4–C yr^{-1}). This is partly related to the difference in lake classifications where in this study lakes were separated by both types and size categories, whereas these previous estimates separated the lakes by type alone-although domain sizes differ slightly. The largest source of lake CH_4 emissions was from small peatland lakes (∼30% of lakes emissions, Table S4), which are dominant in the peat-rich regions of the Hudson Bay Lowlands in Canada and the West Siberian Lowlands in western Russia (Olefeldt et al., 2021). However, the areas of small lakes estimated by BAWLD are among the most uncertain of the land cover classes (Olefeldt et al., 2021) due to limited spatial data used for lakes and great flux variability among small lakes across the domain (Muster et al., 2019). Our mean lake and river CO_2 emission estimates for the permafrost region constitute ∼12% of reported global annual CO_2 emissions for lakes (Holgerson & Raymond, 2016) and rivers (Liu, Kimball, et al., 2022). We note that there is a substantial lack of CH_4 flux data for Boreal-Arctic lakes (Stanley et al., 2016), making our estimates highly uncertain. While there is no estimate of N_2O emissions from arctic lakes, Kortelainen et al. (2020) estimated boreal lakes N_2O emissions at 0.029 (0.026, 0.032) Tg N_2O–N yr^{-1}.

3.3. Net GHG Balance From Disturbances

Fires within the study region affected 1.1×10^6 km^2 during the period 2000–2020. On average, fires impacted 0.06 million km^2 annually, emitting 121 (96.7, 145.3) Tg CO_2–C yr^{-1}, 1.8 (1.4, 2.1) Tg CH_4–C yr^{-1}, and 0.12 (0.10, 0.15) Tg N_2O–N yr^{-1}. Ninety percent of the annually burned area was in the boreal biome, contributing to more than 92% of the permafrost region fire GHG emissions (Table 1). Fire CO_2 emissions offset a third of the CO_2 uptake from terrestrial ecosystems, while CH_4 and N_2O emissions from fires represent 7% and 21% of the CH_4 and N_2O emitted by terrestrial ecosystems, respectively. Our fire emission estimates mainly reflect direct emissions from combustion. There is also a component of increased growth during post-fire recovery, which we do not explicitly account for. However, it is indirectly accounted for as many of the in situ flux data were collected from previously burned ecosystems (which drives up the mean land cover flux). Our fire carbon emission estimate for boreal ecosystems (CO_2 and CH_4, 123 TgC yr^{-1}) is slightly lower than that of 142 Tg CO_2–C yr^{-1} previously reported by Veraverbeke et al. (2021). Using GFED4s data, our estimate might underestimate fire CO_2 emissions, as shown in Potter et al. (2022), where GFED4s emissions were 36% lower than those obtained using the ABoVE-FED data-driven product.

19449224, 2024, 4, Downloaded from https://agupubs.onlinelibrary.wiley.com/doi/10.1029/2023GB007953 by Cochrane France, Wiley Online Library on [08/04/2024]. See the Terms and Conditions (https://onlinelibrary.wiley.com/terms-and-conditions) on Wiley Online Library for rules of use; OA articles are governed by the applicable Creative Commons License

The total area affected by active and stabilized abrupt thaw between 2000 and 2020 was estimated to be 1.2×10^6 km^2 (0.43×10^6 in lowlands, 0.01×10^6 in uplands, and 0.72×10^6 in wetlands), accounting for ca. 7% of the permafrost region (Table 1). Altogether, areas affected by abrupt thaw were net emitters of 31 (21, 42) Tg CO_2–C yr^{-1} and 31 (20, 42) Tg CH_4–C yr^{-1} (Table 1, details in Table S7). CO_2 and CH_4 emissions from wetland abrupt thaw were the largest (Table 1). GHG estimates from abrupt thaw were not directly included in the permafrost GHG balance as it was not possible to know how much were already accounted for in the GHG balance from terrestrial upscaling. However, the impact of abrupt thaw processes on C cycling in the permafrost region is large, and it is projected that it will contribute nearly as much as gradual thaw to future radiative forcing from permafrost thaw (Turetsky et al., 2020).

3.4. Total GHGs, C, and N Budgets

Summing up all budget components, the permafrost region was a source of GHGs throughout the period 2000–2020 (Table 1). Emissions of CO_2 were weak with 12 (−606.4, 661.4) Tg CO_2–C yr^{-1} due to the large CO_2 uptake from terrestrial ecosystems. Emissions from aquatic ecosystems were the largest source of CO_2 annually. CH_4 and N_2O emissions were 38.3 (21.8, 53.4) Tg CH_4–C yr^{-1} and 0.67 (0.07, 1.25) Tg N_2O–N yr^{-1}, respectively, with terrestrial ecosystems as largest contributors (67% and 82%, respectively). Lateral fluxes were 94 (79, 111) Tg C yr^{-1} and 2.6 Tg N yr^{-1} (Table 1), with riverine flux contributing 89% and 79%, respectively.

Taking into account all the above mentioned budget components, the total C (including atmospheric CO_2, CH_4, and lateral fluxes) budget for the permafrost region between 2000 and 2020 was estimated to 144.3 (−505.6, 825.8) Tg C yr^{-1}. Atmospheric CO_2 contributed ca. 8% to the total C released from the region, while atmospheric CH_4 contributed 26.5%. The total N budget for the permafrost region was 3.3 (2.0, 4.8) Tg N yr^{-1}. Most of the (76%) the N released was through lateral fluxes, with coastal erosion releasing 30% of the total N from the region. Atmospheric N_2O from inland waters was negligible, whereas atmospheric N_2O from terrestrial ecosystems represented 17% of the total N released in the permafrost region. Atmospheric N_2O losses due to fires represented 4% of the N in the permafrost region.

3.5. Main Sources of Uncertainty and Research Directions

3.5.1. Limitations in the Number of Observations

A major challenge in the representation of GHG exchange in high-latitude and remote environments relates to limitations in spatial representation, length and quality of observational time series (Pallandt et al., 2022; Virkkala et al., 2018). The synthesis data sets used here to estimate GHG fluxes are the most comprehensive ones currently available and have been significantly growing during the past decade. However, more observations covering the full annual cycles are still needed to improve the representativeness of heterogeneous and underrepresented landscapes and climatic conditions. Specifically, more observations from the Dry Tundra land cover class are needed to verify its GHG sink-source status and from ecosystems experiencing disturbances such as abrupt thaw. CH_4 flux measurements are limited in Boreal Forests, and N_2O flux measurements are scarce for all terrestrial and aquatic ecosystems. Across all the GHG fluxes, measurements in environments with low fluxes are also important to avoid biasing our understanding to hotspot regions. Limitations related to the number of flux measurements could be overcome by increasing in situ and laboratory experiments. This would improve the process-based understanding of fluxes and their response to changes in temperature, moisture, permafrost thaw and other disturbances. Improvements in the reporting of measurements and metadata should be prioritized for a better integration of available data, especially to address reporting of net-zero or negative fluxes. Difficulties in measuring small exchange rates can be overcome by using new technologies based on portable, high-precision laser instruments (e.g., D'Imperio et al., 2017; Juncher Jørgensen et al., 2015). Very recently, such portable high-precision instruments are also becoming available for N_2O, opening possibilities for more numerous and accurate N_2O flux estimates, including the capture of N_2O uptake.

N_2O flux measurements from inland waters are still scarce and ice-out estimates are often missing for CH_4 fluxes. Moreover, seasonally inundated water bodies are not well represented although they might contribute substantially to the release of GHGs in short periods of time.

Estimates of high latitude lateral fluxes of C and N are fairly well constrained in comparison to land-atmosphere GHG fluxes. However, available estimates are provided for the major six largest arctic rivers that represent 50%

19449224, 2024, 4, Downloaded from https://agupubs.onlinelibrary.wiley.com/doi/10.1029/2023GB007953 by Cochrane France, Wiley Online Library on [08/04/2024]. See the Terms and Conditions (https://onlinelibrary.wiley.com/terms-and-conditions) on Wiley Online Library for rules of use; OA articles are governed by the applicable Creative Commons License

of the total area covered by rivers (Speetjens et al., 2023). Although smaller catchments are highly abundant, estimates of GHG fluxes are not well constrained for the permafrost region. Improving this understanding will allow lateral flux integration of these smaller catchments in the main estimates of lateral fluxes from inland waters.

3.5.2. Limitations Related to the Land Cover Classification

Differences in GHG fluxes among land cover classes are large. Therefore, it is crucial to obtain their representation correctly to improve land cover-based GHG flux upscaling. To date, there is no accurate land cover classification of permafrost landscapes (both dry and wet) at a circumpolar scale. We used the BAWLD land cover classification (Olefeldt et al., 2021) in which land cover classes were defined to enable upscaling of CH_4 fluxes at large spatial scales. While very relevant to facilitate large-scale mapping of CH_4 fluxes, it lacks sufficient classes to allow separation among groups of dryer ecosystems that might have large variability in CO_2 or N_2O fluxes. This is the case for the Dry Tundra and Boreal Forest classes that comprise a mosaic of ecosystems with different vegetation types. This results in a large uncertainty range in the class flux estimate of the Dry Tundra (see Table 1, Table S6), making the interpretation of the flux estimates difficult.

Emissions from small water bodies (<0.1 km^2) globally represent important inland water CO_2 and CH_4 fluxes (Holgerson & Raymond, 2016) and even more at high latitudes. Although accounted for in this study, emissions from small water bodies are quite uncertain as they are difficult to map at a large scale due to their high temporal and spatial variability. Small ponds and lakes can be temporary and their size can vary depending on the amount of precipitation after snowmelt; they expand much in wet years and after snowmelt and can often disappear in dry years or late in summer. Improving the spatial and temporal resolution of the products used to map inland waters would benefit the representation of small water bodies, which would resolve a critical source of uncertainty in calculating GHG exchange.

3.5.3. Limited Understanding of the Impact of Disturbances on the GHG Budget

As ecosystems go through disturbance cycles, there are both losses and gains of C and N to ecosystems. It is unclear how well post-disturbance dynamics, for example, post-fire regrowth, is captured in our ecosystem flux upscaling. Our emissions from fires consider direct GHG emissions but not the indirect and longer-term soil emissions resulting from fire-induced ground thaw. Although carbon losses might be offset by shifts in species composition (Mack et al., 2021; Randerson et al., 2006; Ueyama et al., 2019), fires can also initiate further permafrost thaw and degradation (Genet et al., 2013; Gibson et al., 2018; Jafarov et al., 2013). As such, fires can trigger shifts in the landscapes, impacting biogeochemical cycling (Abbott & Jones, 2015; Bouskill et al., 2022; Hermesdorf et al., 2022; Köster, Köster, Berninger, Prokushkin, et al., 2018; Marushchak et al., 2021; Randerson et al., 2006; Ullah et al., 2009; Voigt et al., 2017; Wilkerson et al., 2019). Improving our understanding of landscape transitions due to fire will help constrain the contribution of disturbances to the GHG balance in the region. Next GHG budgets for the permafrost region will need to call for new data sets of fire emissions that account for post-fire recovery processes.

The spatial extent and GHG emissions from abrupt thaw disturbances remain poorly constrained due to a lack of available data (Turetsky et al., 2020). Flux measurements from abrupt thaw are still scarce and thus their reported flux estimate should be interpreted carefully. Improving the number of in situ measurements from abrupt thaw disturbances and consistent reporting should be a key to understanding the impact of abrupt thaw on permafrost GHG budgets. Transition rates (from active to stabilized abrupt thaw feature) need to be further understood and systematic mapping of abrupt thaw areas remain to be improved to better constrain emissions from abrupt thaw. N_2O emissions from abrupt thaw were not included in this study due to the small number of observations reported in the literature and little understanding on the impact of abrupt thaw on emissions N_2O. However, it has been shown that such disturbances frequently cause N_2O emission hotspots (Voigt et al., 2020a). Two recent studies using a terrestrial ecosystem model simulate enhanced gaseous N losses from thawing permafrost (Lacroix et al., 2022; Yuan et al., 2023). Another study showed that uptake of atmospheric N_2O in peat plateaus and thermokarst bogs increased with soil temperature and soil moisture following disturbances (Schulze et al., 2023). Local hydrology will determine whether the site will turn into a source of N_2O after thaw as high emissions can occur at intermediate moisture conditions in N rich soils (Marushchak et al., 2021), but a transition to wetland would promote denitrification with N_2 as the final product and prevent

19449224, 2024, 4, Downloaded from https://agupubs.onlinelibrary.wiley.com/doi/10.1029/2023GB007953 by Cochrane France, Wiley Online Library on [08/04/2024]. See the Terms and Conditions (https://onlinelibrary.wiley.com/terms-and-conditions) on Wiley Online Library for rules of use; OA articles are governed by the applicable Creative Commons License

N_2O release (Butterbach-Bahl & Dannenmann, 2011; Voigt et al., 2017) or even cause or enhance net N_2O uptake (Schulze et al., 2023).

As our understanding of processes leading to GHG release through abrupt thaw is constantly improving, future permafrost GHG budgets will be able to better integrate both atmospheric and lateral fluxes from abrupt thaw. Thus far, the abrupt thaw model (Turetsky et al., 2020) does not consider lateral fluxes from abrupt thaw. While we might capture these losses through our lateral fluxes, future budgets should allow measuring the fraction of what is lost due to abrupt thaw. Other disturbances including anthropogenic disturbances (e.g., clear cutting and logging) have not been estimated in this study. Future budgets could aim at constraining the impact of these disturbances on the permafrost GHG budget.

4. Conclusions

Using a land cover-based ecosystem flux upscaling approach (including fluxes from terrestrial ecosystems, inland water, disturbances and geological fluxes), the permafrost region was identified as an annual source of GHGs between 2000 and 2020. The region emitted 12 (−606, 661) Tg CO_2–C yr^{-1} (mean and 95% confidence interval range used hereafter), 38 (22, 53) Tg CH_4–C yr^{-1}, and 0.67 (0.07, 1.3) Tg N_2O–N yr^{-1} to the atmosphere. The region was thus a net source of CH_4 and N_2O. For CO_2, although the 20-year mean is a net source, the uncertainty range remains large, extending from a large sink to an even larger source of CO_2 and therefore challenging the calculation of the net flux sign. We suggest that terrestrial ecosystems were likely an ecosystem CO_2 sink, but emissions from disturbances and inland waters offset this flux, making the full CO_2 budget largely indistinguishable from zero (neutral). The total C (including atmospheric CO_2, CH_4, and lateral fluxes) and N budgets for the permafrost region were estimated to 144 (−506, 826) Tg C yr^{-1} and 3 (2, 5) Tg N yr^{-1}.

Data Availability Statement

The land cover mean GHG fluxes were obtained for each of the five terrestrial land cover classes after homogenizing and analyzing three comprehensive GHG flux data sets: Virkkala et al. (2022) for CO_2 fluxes; Kuhn et al. (2021a) for CH_4 fluxes; and Voigt et al. (2020a, 2020b) for N_2O fluxes. Additional data were extracted from the literature for Boreal Forest N_2O fluxes (Kim & Tanaka, 2003; Köster, Köster, Berninger, Heinonsalo, & Pumpanen, 2018; Matson et al., 2009; Morishita et al., 2007; Schiller & Hastie, 1996; Simpson et al., 1997; Ullah et al., 2009) since the N_2O flux data set from Voigt et al. (2020b) does not cover Boreal Forest ecosystems. Estimates of river and stream CO_2 flux were calculated from gridded monthly flux data estimated by Liu (2021; https://doi.org/10.5061/dryad.d7wm37pz9; Dryad). Estimates of river N_2O flux were derived from gridded annual N_2O flux estimated by a mechanistic mass balance model developed globally for inland waters by Maavara et al. (2019). CH4 fluxes (diffusion and ebullition) were extracted from the BAWLD-CH4 aquatic ecosystem data set (Kuhn et al., 2021a). Estimated lake CO_2 fluxes were compiled from multiple available sources based on a literature search made in May 2022 (Humborg et al., 2010; Karlsson et al., 2013; Kortelaine et al., 2006; Pelletier et al., 2014; Rasilo et al., 2015; Rocher-Ros et al., 2017; Sepulveda-Jauregui et al., 2015) and are summarized in Table S5). To estimate lake fluxes of N_2O, gridded global data of annual flux from Lauerwald et al. (2019) were used. Monthly GHG fire emissions were extracted for the study region from the Global Fire Emission Database version 4s for the period 1997–2016 and its Beta version for the years 2017–2020 (GFED; van der Werf et al., 2017). We report abrupt thaw areas and derived annual CO_2 and CH_4 emissions using the inventory-based abrupt thaw model by Turetsky et al. (2020). Lateral C and N fluxes from riverine transport and coastal erosion (i.e., dissolved organic carbon and dissolved organic nitrogen losses from the permafrost region to the ocean) are taken from Terhaar et al. (2021). Estimates of geological emissions of CH_4 (from subsurface fossil hydrocarbon reservoirs) are taken from an upscaled circumpolar permafrost region estimate for gas seeps along permafrost boundaries and lake beds made by Walter Anthony et al. (2012).

Acknowledgments
This work is a collaborative effort from the Global Carbon Project Second REgional Carbon Cycle and Processes study (RECCAP2) and contributes to the Arctic Methane and Permafrost Challenge. JR and GH acknowledge support from the European Union's Horizon 2020 Research and Innovation Programme to the Nunataryuk project (no. 773421) and support from the AMPAC-Net project funded by the European Space Agency. JR received additional funding from the Swedish Academy of Science (Formas) under the Grant FR-2021/0004. EJB has received funding from the European Union's Horizon 2020 research and innovation programme under Grant Agreement No 101003536 (ESM2025 - Earth System models for the Future) and from the Joint UK BEIS/Defra Met Office Hadley Centre Climate Programme (GA01101). Work of MEM was supported by the Academy of Finland in the frame of the Atmosphere and Climate Competence Center (no. 337550). CV was supported by the Academy of Finland project MUFFIN (Grant 332196) and the BMBF project MOMENT (no. 03F0931 A). CB wishes to thank the Academy of Finland (project N-PERM - decision no. 341348, project NOCA - decision no. 314630 and the Yedoma-N project decision no. 287469) for financial support. AMV, BMR, SMN, JDW, and SP were funded by the Gordon and Betty Moore foundation (Grant 8414) and through funding catalyzed by the Audacious Project (Permafrost Pathways). MAK was supported by the NSF PRFB Program (Abstract # 2109429). CT acknowledges support through the project Palmod, funded by the German Federal Ministry of Education and Research (BMBF), Grant 01LP1921 A. JGC was funded by the Australian National Environmental Science Program (NESP2) —Climate Systems Hub. MIROC4-ACTM inversion activity is supported by the Arctic Challenge for Sustainability phase II (ArCS-II; JPMXD1420318865) Projects of the Ministry of Education, Culture, Sports, Science and Technology (MEXT), and Environment Research and Technology Development Fund (JPMEERF21S20800) of the Environmental Restoration and Conservation Agency of Japan. ELB considers this study a contribution to GreenFeedBack (Greenhouse gas fluxes and earth system feedbacks) funded by the European Union's HORIZON research and innovation program under grant agreement No 101056921. EAGS was funded by NSF PLR Arctic System Science Research Networking Activities Permafrost Carbon Network: Synthesizing Flux Observations for Benchmarking Model Projections of Permafrost Carbon Exchange (2019–2023) Grant 1931333.

References

Abbott, B. W., & Jones, J. B. (2015). Permafrost collapse alters soil carbon stocks, respiration, CH4, and N2O in upland tundra. *Global Change Biology*, *21*(12), 4570–4587. https://doi.org/10.1111/gcb.13069

Biskaborn, B. K., Smith, S. L., Noetzli, J., Matthes, H., Vieira, G., Streletskiy, D. A., et al. (2019). Permafrost is warming at a global scale. *Nature Communications*, *10*(1), 1–11. https://doi.org/10.1038/s41467-018-08240-4

Bouskill, N. J., Mekonnen, Z., Zhu, Q., Grant, R., & Riley, W. J. (2022). Microbial contribution to post-fire tundra ecosystem recovery over the 21st century. *Communications Earth & Environment*, *3*(1), 26. https://doi.org/10.1038/s43247-022-00356-2

19449224, 2024, 4, Downloaded from https://agupubs.onlinelibrary.wiley.com/doi/10.1029/2023GB007953 by Cochrane France, Wiley Online Library on [08/04/2024]. See the Terms and Conditions (https://onlinelibrary.wiley.com/terms-and-conditions) on Wiley Online Library for rules of use; OA articles are governed by the applicable Creative Commons License

Burke, E., Chadburn, S., & Huntingford, C. (2022). Thawing permafrost as a nitrogen fertiliser: Implications for climate feedbacks. *Nitrogen*, *3*(2), 353–375. https://doi.org/10.3390/nitrogen3020023

Burke, E. J., Ekici, A., Huang, Y., Chadburn, S. E., Huntingford, C., Ciais, P., et al. (2017). Quantifying uncertainties of permafrost carbon–climate feedbacks. *Biogeosciences*, *14*(12), 3051–3066. https://doi.org/10.5194/bg-14-3051-2017

Butterbach-Bahl, K., & Dannenmann, M. (2011). Denitrification and associated soil N_2O emissions due to agricultural activities in a changing climate. *Current Opinion in Environmental Sustainability*, *3*(5), 389–395. https://doi.org/10.1016/j.cosust.2011.08.004

Chadburn, S., Burke, E., Cox, P., Friedlingstein, P., Hugelius, G., & Westermann, S. (2017). An observation-based constraint on permafrost loss as a function of global warming. *Nature Climate Change*, *7*(5), 340–344. https://doi.org/10.1038/nclimate3262

Chen, Y., Liu, F., Kang, L., Zhang, D., Kou, D., Mao, C., et al. (2021). Large-scale evidence for microbial response and associated carbon release after permafrost thaw. *Global Change Biology*, *27*(14), 3218–3229. https://doi.org/10.1111/gcb.15487

Ciais, P., Bastos, A., Chevallier, F., Lauerwald, R., Poulter, B., Canadell, P., et al. (2022). Definitions and methods to estimate regional land carbon fluxes for the second phase of the REgional Carbon Cycle Assessment and Processes Project (RECCAP-2). *Geoscientific Model Development*, *15*(3), 1289–1316. https://doi.org/10.5194/gmd-15-1289-2022

Cole, J. J., Prairie, Y. T., Caraco, N. F., McDowell, W. H., Tranvik, L. J., Striegl, R. G., et al. (2007). Plumbing the global carbon cycle: Integrating inland waters into the terrestrial carbon budget. *Ecosystems*, *10*(1), 172–185. https://doi.org/10.1007/s10021-006-9013-8

Denfeld, B. A., Baulch, H. M., del Giorgio, P. A., Hampton, S. E., & Karlsson, J. (2018). A synthesis of carbon dioxide and methane dynamics during the ice-covered period of northern lakes. *Limnology and Oceanography Letters*, *3*(3), 117–131. https://doi.org/10.1002/lol2.10079

D'Imperio, L., Li, B. B., Tiedje, J. M., Oh, Y., Christiansen, J. R., Kepfer-Rojas, S., et al. (2023). Spatial controls of methane uptake in upland soils across climatic and geological regions in Greenland. *Communications Earth & Environment*, *4.1*(1), 461. https://doi.org/10.1038/s43247-023-01143-3

D'Imperio, L., Nielsen, C. S., Westergaard-Nielsen, A., Michelsen, A., & Elberling, B. (2017). Methane oxidation in contrasting soil types: Responses to experimental warming with implication for landscape-integrated CH4 budget. *Global Change Biology*, *23*(2), 966–976. https://doi.org/10.1111/gcb.13400

Genet, H., McGuire, A. D., Barrett, K., Breen, A., Euskirchen, E. S., Johnstone, J. F., et al. (2013). Modeling the effects of fire severity and climate warming on active layer thickness and soil carbon storage of black spruce forests across the landscape in interior Alaska. *Environmental Research Letters*, *8*(4), 045016. https://doi.org/10.1088/1748-9326/8/4/045016

Gibson, C. M., Chasmer, L. E., Thompson, D. K., Quinton, W. L., Flannigan, M. D., & Olefeldt, D. (2018). Wildfire as a major driver of recent permafrost thaw in boreal peatlands. *Nature Communications*, *9*(1), 3041. https://doi.org/10.1038/s41467-018-05457-1

Gil, J., Marushchak, M. E., Rütting, T., Baggs, E. M., Pérez, T., Novakovskiy, A., et al. (2022). Sources of nitrous oxide and the fate of mineral nitrogen in subarctic permafrost peat soils. *Biogeosciences*, *19*(10), 2683–2698.

Grosse, G., Harden, J., Turetsky, M., McGuire, A. D., Camill, P., Tarnocai, C., et al. (2011). Vulnerability of high-latitude soil organic carbon in North America to disturbance. *Journal of Geophysical Research*, *116*(G4), G00K06. https://doi.org/10.1029/2010jg001507

Hermesdorf, L., Elberling, B., D'Imperio, L., Xu, W., Lambæk, A., & Ambus, P. L. (2022). Effects of fire on CO2, CH4 and N2O exchange in a well-drained Arctic heath ecosystem. *Global Change Biology*.

Holgerson, M. A., & Raymond, P. A. (2016). Large contribution to inland water CO_2 and CH_4 emissions from very small ponds. *Nature Geoscience*, *9*(3), 222–226. https://doi.org/10.1038/ngeo2654

Holloway, J. E., Lewkowicz, A. G., Douglas, T. A., Li, X., Turetsky, M. R., Baltzer, J. L., & Jin, H. (2020). Impact of wildfire on permafrost landscapes: A review of recent advances and future prospects. *Permafrost and Periglacial Processes*, *31*(3), 371–382. https://doi.org/10.1002/ppp.2048

Hugelius, G., Ramage, J. L., Burke, E. J., Chatterjee, A., Smallman, T. L., Aalto, T., et al. (2023). Two decades of permafrost region CO2, CH4, and N2O budgets suggest a small net greenhouse gas source to the atmosphere. *ESS Open Archive*. https://doi.org/10.22541/essoar.169444320.01914726/v1

Hugelius, G., Strauss, J., Zubrzycki, S., Harden, J. W., Schuur, E. A., Ping, C. L., et al. (2014). Estimated stocks of circumpolar permafrost carbon with quantified uncertainty ranges and identified data gaps. *Biogeosciences*, *11*(23), 6573–6593. https://doi.org/10.5194/bg-11-6573-2014

Humborg, C., Mörth, C. M., Sundbom, M., Borg, H., Blenckner, T., Giesler, R., & Ittekkot, V. (2010). CO2 supersaturation along the aquatic conduit in Swedish watersheds as constrained by terrestrial respiration, aquatic respiration and weathering. *Global Change Biology*, *16*(7), 1966–1978. https://doi.org/10.1111/j.1365-2486.2009.02092.x

Jafarov, E. E., Romanovsky, V. E., Genet, H., McGuire, A. D., & Marchenko, S. S. (2013). The effects of fire on the thermal stability of permafrost in lowland and upland black spruce forests of interior Alaska in a changing climate. *Environmental Research Letters*, *8*(3), 035030. https://doi.org/10.1088/1748-9326/8/3/035030

Juncher Jørgensen, C., Lund Johansen, K. M., Westergaard-Nielsen, A., & Elberling, B. (2015). Net regional methane sink in High Arctic soils of northeast Greenland. *Nature Geoscience*, *8*(1), 20–23. https://doi.org/10.1038/ngeo2305

Karlsson, J., Giesler, R., Persson, J., & Lundin, E. (2013). High emission of carbon dioxide and methane during ice thaw in high latitude lakes. *Geophysical Research Letters*, *40*(6), 1123–1127. https://doi.org/10.1002/grl.50152

Kim, Y., & Tanaka, N. (2003). Effect of forest fire on the fluxes of CO2, CH4, and N2O in boreal forest soils, interior Alaska. *Journal of Geophysical Research*, *108*(D1), 8154. https://doi.org/10.1029/2001JD000663

Kortelainen, P., Larmola, T., Rantakari, M., Juutinen, S., Alm, J., & Martikainen, P. J. (2020). Lakes as nitrous oxide sources in the boreal landscape. *Global Change Biology*, *26*(3), 1432–1445. https://doi.org/10.1111/gcb.14928

Kortelainen, P., Rantakari, M., Huttunen, J. T., Mattsson, T., Alm, J., Juutinen, S., et al. (2006). Sediment respiration and lake trophic state are important predictors of large CO_2 evasion from small boreal lakes. *Global Change Biology*, *12*(8), 1554–1567. https://doi.org/10.1111/j.1365-2486.2006.01167.x

Köster, E., Köster, K., Berninger, F., Prokushkin, A., Aaltonen, H., Zhou, X., & Pumpanen, J. (2018). Changes in fluxes of carbon dioxide and methane caused by fire in Siberian boreal forest with continuous permafrost. *Journal of Environmental Management*, *228*, 405–415. https://doi.org/10.1016/j.jenvman.2018.09.051

Köster, K., Köster, E., Berninger, F., Heinonsalo, J., & Pumpanen, J. (2018). Contrasting effects of reindeer grazing on CO2, CH4, and N2O fluxes originating from the northern boreal forest floor. *Land Degradation & Development*, *29*(2), 374–381. https://doi.org/10.1002/ldr.2868

Koven, C. D., Schuur, E. A. G., Schädel, C., Bohn, T. J., Burke, E. J., Chen, G., et al. (2015). A simplified, data-constrained approach to estimate the permafrost carbon–climate feedback. *Philosophical Transactions of the Royal Society A: Mathematical, Physical & Engineering Sciences*, *373*(2054), 20140423. https://doi.org/10.1098/rsta.2014.0423

Kuhn, M. A., Thompson, L. M., Winder, J. C., Braga, L. P., Tanentzap, A. J., Bastviken, D., & Olefeldt, D. (2021c). Opposing effects of climate and permafrost thaw on CH4 and CO2 emissions from northern lakes. *AGU Advances*, *2*(4), e2021AV000515. https://doi.org/10.1029/2021av000515

19449224, 2024, 4, Downloaded from https://agupubs.onlinelibrary.wiley.com/doi/10.1029/2023GB007953 by Cochrane France, Wiley Online Library on [08/04/2024]. See the Terms and Conditions (https://onlinelibrary.wiley.com/terms-and-conditions) on Wiley Online Library for rules of use; OA articles are governed by the applicable Creative Commons License

Kuhn, M. A., Thompson, L. M., Winder, J. C., Braga, L. P. P., Tanentzap, A. J., Bastviken, D., & Olefeldt, D. (2021). b. Opposing effects of climate and permafrost thaw on CH4 and CO2 emissions from northern lakes. *AGU Advances*, *2*(4), e2021AV000515. https://doi.org/10.1029/2021AV000515

Kuhn, M. A., Varner, R. K., Bastviken, D., Crill, P., MacIntyre, S., Turetsky, M., et al. (2021a). BAWLD-CH4: A comprehensive dataset of methane fluxes from boreal and arctic ecosystems. *Earth System Science Data Discussions*, *13*(11), 1–56. https://doi.org/10.5194/essd-13-5151-2021

Lacroix, F., Zaehle, S., Caldararu, S., Schaller, J., Stimmler, P., Holl, D., et al. (2022). Mismatch of N release from the permafrost and vegetative uptake opens pathways of increasing nitrous oxide emissions in the high Arctic. *Global Change Biology*, *28*(20), 5973–5990. https://doi.org/10.1111/gcb.16345

Lantuit, H., Overduin, P. P., Couture, N., Wetterich, S., Aré, F., Atkinson, D., et al. (2012). The Arctic Coastal Dynamics database: A new classification scheme and statistics on Arctic permafrost coastlines. *Estuaries and Coasts*, *35*(2), 383–400. https://doi.org/10.1007/s12237-010-9362-6

Lauerwald, R., Regnier, P., Figueiredo, V., Enrich-Prast, A., Bastviken, D., Lehner, B., et al. (2019). Natural lakes are a minor global source of N2O to the atmosphere. *Global Biogeochemical Cycles*, *33*(12), 1564–1581. https://doi.org/10.1029/2019GB006261

Lee, J., Oh, Y., Lee, S. T., Seo, Y. O., Yun, J., Yang, Y., et al. (2023). Soil organic carbon is a key determinant of CH_4 sink in global forest soils. *Nature Communications*, *14*(1), 3110. https://doi.org/10.1038/s41467-023-38905-8

Li, G., Zhang, M., Pei, W., Melnikov, A., Khristoforov, I., Li, R., & Yu, F. (2022). Changes in permafrost extent and active layer thickness in the Northern Hemisphere from 1969 to 2018. *Science of the Total Environment*, *804*, 150182. https://doi.org/10.1016/j.scitotenv.2021.150182

Liu, S. (2021). Monthly pCO2, gas transfer velocity and CO2 efflux rate in global streams and rivers (the GRADES river networks) [Dataset]. *Dryad*. https://doi.org/10.5061/dryad.d7wm37pz9

Liu, S., Kuhn, C., Amatulli, G., Aho, K., Butman, D. E., Allen, G. H., et al. (2022). The importance of hydrology in routing terrestrial carbon to the atmosphere via global streams and rivers. *Proceedings of the National Academy of Sciences*, *119*(11), e2106322119. https://doi.org/10.1073/pnas.2106322119

Liu, Z., Kimball, J. S., Ballantyne, A. P., Parazoo, N. C., Wang, W. J., Bastos, A., et al. (2022). Respiratory loss during late-growing season determines the net carbon dioxide sink in northern permafrost regions. *Nature Communications*, *13*(1), 1–13. https://doi.org/10.1038/s41467-022-33293-x

López-Blanco, E., Langen, P. L., Williams, M., Christensen, J. H., Boberg, F., Langley, K., & Christensen, T. R. (2022). The future of tundra carbon storage in Greenland – Sensitivity to climate and plant trait changes. *Science of the Total Environment*, 157385. https://doi.org/10.1016/j.scitotenv.2022

Maavara, T., Lauerwald, R., Laruelle, G., Akbarzadeh, Z., Bouskill, N., Van Cappellen, P., & Regnier, P. (2019). Nitrous oxide emissions from inland waters: Are IPCC estimates too high? *Global Change Biology*, *25*(2), 473–488. https://doi.org/10.1111/gcb.14504

Mack, M. C., Walker, X. J., Johnstone, J. F., Alexander, H. D., Melvin, A. M., Jean, M., & Miller, S. N. (2021). Carbon loss from boreal forest wildfires offset by increased dominance of deciduous trees. *Science*, *372*(6539), 280–283. https://doi.org/10.1126/science.abf3903

Marushchak, M. E., Kerttula, J., Diáková, K., Faguet, A., Gil, J., Grosse, G., et al. (2021). Thawing Yedoma permafrost is a neglected nitrous oxide source. *Nature Communications*, *12*(1), 7107. https://doi.org/10.1038/s41467-021-27386-2

Marushchak, M. E., Pitkämäki, A., Koponen, H., Biasi, C., Seppälä, M., & Martikainen, P. J. (2011). Hot spots for nitrous oxide emissions found in different types of permafrost peatlands. *Global Change Biology*, *17*(8), 2601–2614. https://doi.org/10.1111/j.1365-2486.2011.02442.x

Matson, A., Pennock, D., & Bedard-Haughn, A. (2009). Methane and nitrous oxide emissions from mature forest stands in the boreal forest, Saskatchewan, Canada. *Forest Ecology and Management*, *258*(7), 1073–1083. https://doi.org/10.1016/j.foreco.2009.05.034

Matthews, E., Johnson, M. S., Genovese, V., Du, J., & Bastviken, D. (2020). Methane emission from high latitude lakes: Methane-centric lake classification and satellite-driven annual cycle of emissions. *Scientific Reports*, *10*(1), 1–9. https://doi.org/10.1038/s41598-020-68246-1

McGuire, A. D., Christensen, T. R., Hayes, D., Heroult, A., Euskirchen, E., Kimball, J. S., et al. (2012). An assessment of the carbon balance of Arctic tundra: Comparisons among observations, process models, and atmospheric inversions. *Biogeosciences*, *9*(8), 3185–3204. https://doi.org/10.5194/bg-9-3185-2012

McGuire, A. D., Lawrence, D. M., Koven, C., Clein, J. S., Burke, E., Chen, G., et al. (2018). Dependence of the evolution of carbon dynamics in the northern permafrost region on the trajectory of climate change. *Proceedings of the National Academy of Sciences of the United States of America*, *115*(15), 3882–3887. https://doi.org/10.1073/pnas.1719903115

Mishra, U., Hugelius, G., Shelef, E., Yang, Y., Strauss, J., Lupachev, A., et al. (2021). Spatial heterogeneity and environmental predictors of permafrost region soil organic carbon stocks. *Science Advances*, *7*(9), eaaz5236. https://doi.org/10.1126/sciadv.aaz5236

Morishita, T., Hatano, R., & Desyatkin, R. V. (2007). N2O flux in Alas ecosystems formed by forest disturbance near Yakutsk, Eastern Siberia, Russia. *Eurasian Journal of Forest Research*, *10*(1), 79–84.

Mörner, N.-A., & Etiope, G. (2002). Carbon degassing from the lithosphere, Global Planet. *Change*, *33*(1–2), 185–203. https://doi.org/10.1016/s0921-8181(02)00070-x

Muster, S., Riley, W. J., Roth, K., Langer, M., Cresto Aleina, F., Koven, C. D., et al. (2019). Size distributions of Arctic waterbodies reveal consistent relations in their statistical moments in space and time. *Frontiers in Earth Science*, *7*, 5. https://doi.org/10.3389/feart.2019.00005

Natali, S. M., Watts, J. D., Rogers, B. M., Potter, S., Ludwig, S. M., Selbmann, A. K., et al. (2019). Large loss of CO2 in winter observed across the northern permafrost region. *Nature Climate Change*, *9*(11), 852–857. https://doi.org/10.1038/s41558-019-0592-8

Obu, J., Westermann, S., Barboux, C., Bartsch, A., Delaloye, R., Grosse, G., et al. (2021). *ESA permafrost climate change initiative (Permafrost_cci): Permafrost extent for the Northern Hemisphere, v3.0*. NERC EDS Centre for Environmental Data Analysis. https://doi.org/10.5285/6e2091cb0c8b4106921b63cd5357c97c

Oh, Y., Zhuang, Q., Liu, L., Welp, L. R., Lau, M. C. Y., Onstott, T. C., et al. (2020). Reduced net methane emissions due to microbial methane oxidation in a warmer Arctic. *Nature Climate Change*, *10.4*(4), 317–321. https://doi.org/10.1038/s41558-020-0734-z

Olefeldt, D., Hovemyr, M., Kuhn, M. A., Bastviken, D., Bohn, T. J., Connolly, J., et al. (2021). The boreal–Arctic wetland and lake dataset (BAWLD). *Earth System Science Data*, *13*(11), 5127–5149. https://doi.org/10.5194/essd-13-5127-2021

Pallandt, M. M., Kumar, J., Mauritz, M., Schuur, E. A., Virkkala, A. M., Celis, G., et al. (2022). Representativeness assessment of the pan-Arctic eddy covariance site network and optimized future enhancements. *Biogeosciences*, *19*(3), 559–583. https://doi.org/10.5194/bg-19-559-2022

Palmtag, J., Obu, J., Kuhry, P., Richter, A., Siewert, M. B., Weiss, N., et al. (2022). A high-spatial resolution soil carbon and nitrogen dataset for the northern permafrost region, based on circumpolar land cover upscaling. *Earth System Science Data Discussions*, *14*(9), 1–28. https://doi.org/10.5194/essd-14-4095-2022

Pelletier, L., Strachan, I. B., Garneau, M., & Roulet, N. T. (2014). Carbon release from boreal peatland open water pools: Implication for the contemporary C exchange. *Journal of Geophysical Research: Biogeosciences*, *119*(3), 207–222. https://doi.org/10.1002/2013jg002423

19449224, 2024, 4, Downloaded from https://agupubs.onlinelibrary.wiley.com/doi/10.1029/2023GB007953 by Cochrane France, Wiley Online Library on [08/04/2024]. See the Terms and Conditions (https://onlinelibrary.wiley.com/terms-and-conditions) on Wiley Online Library for rules of use; OA articles are governed by the applicable Creative Commons License

Peltola, O., Vesala, T., Gao, Y., Räty, O., Alekseychik, P., Aurela, M., et al. (2019). Monthly gridded data product of northern wetland methane emissions based on upscaling eddy covariance observations. *Earth System Science Data*, *11*(3), 1263–1289. https://doi.org/10.5194/essd-11-1263-2019

Potter, S., Cooperdock, S., Veraverbeke, S., Walker, X., Mack, M. C., Goetz, S. J., et al. (2022). *Burned area and carbon emissions across northwestern boreal north America from 2001–2019*. EGUsphere. https://doi.org/10.5194/egusphere-2022-364

Randerson, J. T., Liu, H., Flanner, M. G., Chambers, S. D., Jin, Y., Hess, P. G., et al. (2006). The impact of boreal forest fire on climate warming. *Science*, *314*(5802), 1130–1132. https://doi.org/10.1126/science.1132075

Rantanen, M., Karpechko, A. Y., Lipponen, A., Nordling, K., Hyvärinen, O., Ruosteenoja, K., et al. (2022). The Arctic has warmed nearly four times faster than the globe since 1979. *Communications Earth & Environment*, *3*(1), 168. https://doi.org/10.1038/s43247-022-00498-3

Rasilo, T., Prairie, Y. T., & Del Giorgio, P. A. (2015). Large-scale patterns in summer diffusive CH 4 fluxes across boreal lakes, and contribution to diffusive C emissions. *Global Change Biology*, *21*(3), 1124–1139. https://doi.org/10.1111/gcb.12741

Repo, M. E., Susiluoto, S., Lind, S. E., Jokinen, S., Elsakov, V., Biasi, C., et al. (2009). Large N_2O emissions from cryoturbated peat soil in tundra. *Nature Geoscience*, *2*(3), 189–192. https://doi.org/10.1038/ngeo434

Rocher-Ros, G., Giesler, R., Lundin, E., Salimi, S., Jonsson, A., & Karlsson, J. (2017). Large lakes dominate CO2 evasion from lakes in an Arctic catchment. *Geophysical Research Letters*, *44*(24), 12–254. https://doi.org/10.1002/2017gl076146

Runge, A., Nitze, I., & Grosse, G. (2022). Remote sensing annual dynamics of rapid permafrost thaw disturbances with LandTrendr. *Remote Sensing of Environment*, *268*, 112752. https://doi.org/10.1016/j.rse.2021.112752

Saunois, M., Stavert, A. R., Poulter, B., Bousquet, P., Canadell, J. G., Jackson, R. B., et al. (2019). The global methane budget 2000–2017. *Earth System Science Data Discussions*, 1–136.

Schiller, C. L., & Hastie, D. R. (1996). Nitrous oxide and methane fluxes from perturbed and unperturbed boreal forest sites in northern Ontario. *Journal of Geophysical Research*, *101*(D17), 22767–22774. https://doi.org/10.1029/96JD01620

Schulze, C., Sonnentag, O., Voigt, C., Thompson, L., van Delden, L., Heffernan, L., et al. (2023). Nitrous oxide fluxes in permafrost peatlands remain negligible after wildfire and thermokarst disturbance. *Journal of Geophysical Research: Biogeosciences*, *128*(4), e2022JG007322. https://doi.org/10.1029/2022JG007322

Schuur, E. A. G., Abbott, B., Commane, R., Ernakovich, J., Euskirchen, E., Hugelius, G., et al. (2022). Permafrost and climate change: Carbon cycle feedbacks from a warming Arctic. *Annual Review of Environment and Resources*, *47*, 28.1–28.29. https://doi.org/10.1146/annurev-environ-012220-011847

Schuur, E. A. G., Abbott, B. W., Bowden, W. B., Brovkin, V., Camill, P., Canadell, J. P., et al. (2011). High risk of permafrost thaw. *Nature*, *480*(7375), 32–33. https://doi.org/10.1038/480032a

Schuur, E. A. G., Bockheim, J., Canadell, J., Euskirchen, E., Field, C. B., Goryachkin, S. V., et al. (2008). Vulnerability of permafrost carbon to climate change: Implications for the global carbon cycle. *BioScience*, *58*(8), 701–714. https://doi.org/10.1641/b580807

Schuur, E. A. G., & Mack, M. C. (2018). Ecological response to permafrost thaw and consequences for local and global ecosystem services. *Annual Review of Ecology, Evolution and Systematics*, *49*(1), 279–301. https://doi.org/10.1146/annurev-ecolsys-121415-032349

Schuur, E. A. G., McGuire, A. D., Grosse, G., Harden, J. W., Hayes, D. J., Hugelius, G., et al. (2015). Climate change and the permafrost carbon feedback. *Nature*, *520*(7546), 171–179. https://doi.org/10.1038/nature14338

Schuur, E. A. G., Vogel, J. G., Crummer, K. G., Lee, H., Sickman, J. O., & Osterkamp, T. E. (2009). The effect of permafrost thaw on old carbon release and net carbon exchange from tundra. *Nature*, *459*(7246), 556–559. https://doi.org/10.1038/nature08031

Sepulveda-Jauregui, A., Walter Anthony, K. M., Martinez-Cruz, K., Greene, S., & Thalasso, F. (2015). Methane and carbon dioxide emissions from 40 lakes along a north–south latitudinal transect in Alaska. *Biogeosciences*, *12*(11), 3197–3223. https://doi.org/10.5194/bg-12-3197-2015

Serikova, S., Pokrovsky, O. S., Ala-Aho, P., Kazantsev, V., Kirpotin, S. N., Kopysov, S. G., et al. (2018). High riverine CO2 emissions at the permafrost boundary of Western Siberia. *Nature Geoscience*, *11*, 825–829. https://doi.org/10.1038/s41561-018-0218-1

Simpson, I. J., Edwards, G. C., Thurtell, G. W., den Hartog, G., Neumann, H. H., & Staebler, R. M. (1997). Micrometeorological measurements of methane and nitrous oxide exchange above a boreal aspen forest. *Journal of Geophysical Research*, *102*(D24), 29331–29341. https://doi.org/10.1029/97JD03181

Speetjens, N. J., Hugelius, G., Gumbricht, T., Lantuit, H., Berghuijs, W. R., Pika, P. A., et al. (2023). The pan-Arctic catchment database (ARCADE). *Earth System Science Data*, *15*(2), 541–554. https://doi.org/10.5194/essd-15-541-2023

Stanley, E. H., Casson, N. J., Christel, S. T., Crawford, J. T., Loken, L. C., & Oliver, S. K. (2016). The ecology of methane in streams and rivers: Patterns, controls, and global significance. *Ecological Monographs*, *86*(2), 146–171. https://doi.org/10.1890/15-1027

Tarnocai, C., Canadell, J. G., Schuur, E. A., Kuhry, P., Mazhitova, G., & Zimov, S. (2009). Soil organic carbon pools in the northern circumpolar permafrost region. *Global Biogeochemical Cycles*, *23*(2). https://doi.org/10.1029/2008gb003327

Terhaar, J., Lauerwald, R., Regnier, P., Gruber, N., & Bopp, L. (2021). Around one third of current Arctic Ocean primary production sustained by rivers and coastal erosion. *Nature Communications*, *12*(1), 169. https://doi.org/10.1038/s41467-020-20470-z

Thornton, B. F., Wik, M., & Crill, P. M. (2016). Double-counting challenges the accuracy of high-latitude methane inventories. *Geophysical Research Letters*, *43*(24), 12569–12577. https://doi.org/10.1002/2016GL071772

Treat, C. C., Bloom, A. A., & Marushchak, M. E. (2018). Nongrowing season methane emissions – A significant component of annual emissions across northern ecosystems. *Global Change Biology*, *24*(8), 3331–3343. https://doi.org/10.1111/gcb.14137

Turetsky, M. R., Abbott, B. W., Jones, M. C., Anthony, K. W., Olefeldt, D., Schuur, E. A. G., et al. (2020). Carbon release through abrupt permafrost thaw. *Nature Geoscience*, *13*(2), 138–143. https://doi.org/10.1038/s41561-019-0526-0

Ueyama, M., Iwata, H., Nagano, H., Tahara, N., Iwama, C., & Harazono, Y. (2019). Carbon dioxide balance in early-successional forests after forest fires in interior Alaska. *Agricultural and Forest Meteorology*, *275*, 196–207. https://doi.org/10.1016/j.agrformet.2019.05.020

Ullah, S., Frasier, R., Pelletier, L., & Moore, T. R. (2009). Greenhouse gas fluxes from boreal forest soils during the snow-free period in Quebec, Canada. *Canadian Journal of Forest Research*, *39*(3), 666–680. https://doi.org/10.1139/x08-209

van der Werf, G. R., Randerson, J. T., Giglio, L., van Leeuwen, T. T., Chen, Y., Rogers, B. M., et al. (2017). Global fire emissions estimates during 1997–2016. *Earth System Science Data*, *9*(2), 697–720. https://doi.org/10.5194/essd-9-697-2017

van Wees, D., van der Werf, G. R., Randerson, J. T., Rogers, B. M., Chen, Y., Veraverbeke, S., et al. (2022). Global biomass burning fuel consumption and emissions at 500 m spatial resolution based on the Global Fire Emissions Database (GFED). *Geoscientific Model Development*, *15*(22), 8411–8437. https://doi.org/10.5194/gmd-15-8411-2022

Veraverbeke, S., Delcourt, C. J., Kukavskaya, E., Mack, M., Walker, X., Hessilt, T., et al. (2021). Direct and longer-term carbon emissions from arctic-boreal fires: A short review of recent advances. *Current Opinion in Environmental Science & Health*, *23*, 100277. https://doi.org/10.1016/j.coesh.2021.100277

19449224, 2024, 4, Downloaded from https://agupubs.onlinelibrary.wiley.com/doi/10.1029/2023GB007953 by Cochrane France, Wiley Online Library on [08/04/2024]. See the Terms and Conditions (https://onlinelibrary.wiley.com/terms-and-conditions) on Wiley Online Library for rules of use; OA articles are governed by the applicable Creative Commons License

Virkkala, A.-M., Aalto, J., Rogers, B. M., Tagesson, T., Treat, C. C., Natali, S. M., et al. (2021). Statistical upscaling of ecosystem CO2 fluxes across the terrestrial tundra and boreal domain: Regional patterns and uncertainties. *Global Change Biology*, *27*(17), 4040–4059. https://doi.org/10.1111/gcb.15659

Virkkala, A.-M., Natali, S. M., Rogers, B. M., Watts, J. D., Savage, K., Connon, S. J., et al. (2022). The ABCflux database: Arctic–boreal CO2 flux observations and ancillary information aggregated to monthly time steps across terrestrial ecosystems. *Earth System Science Data*, *14*(1), 179–208. https://doi.org/10.5194/essd-14-179-2022

Virkkala, A.-M., Virtanen, T., Lehtonen, A., Rinne, J., & Luoto, M. (2018). The current state of CO2 flux chamber studies in the Arctic tundra: A review. *Progress in Physical Geography: Earth and Environment*, *42*(2), 162–184. https://doi.org/10.1177/0309133317745784

Voigt, C., Marushchak, M. E., Abbott, B. W., Biasi, C., Elberling, B., Siciliano, S. D., et al. (2020a). Nitrous oxide emissions from permafrost-affected soils. *Nature Reviews Earth & Environment*, *1*(8), 420–434. https://doi.org/10.1038/s43017-020-0063-9

Voigt, C., Marushchak, M. E., Lamprecht, R. E., Jackowicz-Korczyński, M., Lindgren, A., Mastepanov, M., et al. (2017). Increased nitrous oxide emissions from Arctic peatlands after permafrost thaw. *Proceedings of the National Academy of Sciences*, *114*(24), 6238–6243. https://doi.org/10.1073/pnas.1702902114

Voigt, C., van Delden, L., Marushchak, M. E., Biasi, C., Abbott, B. W., Elberling, B., et al. (2020b). Nitrous oxide fluxes from permafrost regions. *PANGAEA*. https://doi.org/10.1594/PANGAEA.919217

Voigt, C., Virkkala, A. M., Hould Gosselin, G., Bennett, K. A., Black, T. A., Detto, M., et al. (2023). Arctic soil methane sink increases with drier conditions and higher ecosystem respiration. *Nature Climate Change*, *13.10*(10), 1095–1104. https://doi.org/10.1038/s41558-023-01785-3

Walker, X. J., Baltzer, J. L., Cumming, S. G., Day, N. J., Ebert, C., Goetz, S., et al. (2019). Increasing wildfires threaten historic carbon sink of boreal forest soils. *Nature*, *572*(7770), 520–523. https://doi.org/10.1038/s41586-019-1474-y

Walter Anthony, K. M., Anthony, P., Grosse, G., & Chanton, J. (2012). Geologic methane seeps along boundaries of Arctic permafrost thaw and melting glaciers. *Nature Geoscience*, *5*(6), 419–426. https://doi.org/10.1038/ngeo1480

Watts, J. D., Farina, M., Kimball, J. S., Schiferl, L. D., Liu, Z., Arndt, K. A., et al. (2023). Carbon uptake in Eurasian boreal forests dominates the high-latitude net ecosystem carbon budget. *Global Change Biology*, *29*(7), 1870–1889. https://doi.org/10.1111/gcb.16553

Whalen, S. C., Reeburgh, W. S., & Barber, V. A. (1992). Oxidation of methane in boreal forest soils – A comparison of 7 measures. *Biogeochemistry*, *16*(3), 181–211. https://doi.org/10.1007/bf00002818

Wik, M., Varner, R. K., Anthony, K. W., MacIntyre, S., & Bastviken, D. (2016). Climate-sensitive northern lakes and ponds are critical components of methane release. *Nature Geoscience*, *9*(2), 99–105. https://doi.org/10.1038/ngeo2578

Wilkerson, J., Dobosy, R., Sayres, D. S., Healy, C., Dumas, E., Baker, B., & Anderson, J. G. (2019). Permafrost nitrous oxide emissions observed on a landscape scale using the airborne eddy-covariance method. *Atmospheric Chemistry and Physics*, *19*(7), 4257–4268. https://doi.org/10.5194/acp-19-4257-2019

Yang, G., Peng, Y., Marushchak, M. E., Chen, Y., Wang, G., Li, F., et al. (2018). Magnitude and pathways of increased nitrous oxide emissions from uplands following permafrost thaw. *Environmental Science & Technology*, *52*(16), 9162–9169. https://doi.org/10.1021/acs.est.8b02271

Yuan, Y., Zhuang, Q., Zhao, B., & Shurpali, N. (2023). Nitrous oxide emissions from pan-Arctic terrestrial ecosystems: A process-based biogeochemistry model analysis from 1969 to 2019. *EGUsphere*. [preprint]. https://doi.org/10.5194/egusphere-2023-1047

19449224, 2024, 4, Downloaded from https://agupubs.onlinelibrary.wiley.com/doi/10.1029/2023GB007953 by Cochrane France, Wiley Online Library on [08/04/2024]. See the Terms and Conditions (https://onlinelibrary.wiley.com/terms-and-conditions) on Wiley Online Library for rules of use; OA articles are governed by the applicable Creative Commons License